

CHARACTERIZATION AND MAGNETIZATION STUDIES ON COPRECIPITATED BARIUM HEXAFERRITE

A Thesis Submitted
In Partial Fulfilment of the Requirements
for the Degree of
MASTER OF TECHNOLOGY

by
SUJOY BHATTACHARYYA

to the
DEPARTMENT OF METALLURGICAL ENGINEERING

INDIAN INSTITUTE OF TECHNOLOGY, KANPUR
AUGUST, 1988

CHARACTERIZATION AND MAGNETIZATION STUDIES ON COPRECIPITATED BARIUM HEXAFERRITE

A Thesis Submitted
In Partial Fulfilment of the Requirements
for the Degree of
MASTER OF TECHNOLOGY

by
SUJOY BHATTACHARYYA

to the
DEPARTMENT OF METALLURGICAL ENGINEERING

INDIAN INSTITUTE OF TECHNOLOGY, KANPUR
AUGUST, 1988

CHARACTERIZATION AND MAGNETIZATION STUDIES ON COPRECIPITATED BARIUM HEXAFERRITE

A Thesis Submitted
In Partial Fulfilment of the Requirements
for the Degree of
MASTER OF TECHNOLOGY

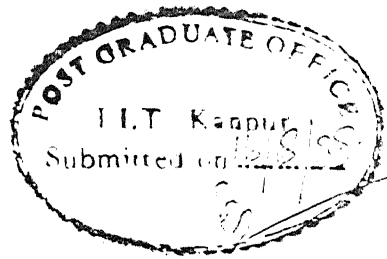
by
SUJOY BHATTACHARYYA

to the
DEPARTMENT OF METALLURGICAL ENGINEERING

INDIAN INSTITUTE OF TECHNOLOGY, KANPUR
AUGUST, 1988

20 APR 1989
CENTRAL LIBRARY
I.I.T., KANPUR
Acc. No. A.104246

ME-1980-M-BHA-CHA

CERTIFICATE

Certified that the thesis entitled "Characterization and Magnetization Studies on Coprecipitated Barium Hexaferrite" has been carried out under my supervision and it has not been submitted elsewhere for a degree.

A. R. Das
Professor

August, 1988

Department of Metallurgical Engineering
Indian Institute of Technology
Kanpur.

ACKNOWLEDGEMENTS

I take this opportunity to express my hearty gratitude to Dr. A.R. Das for suggesting this topic and for his constant guidance and encouragement throughout the course of this work.

I gratefully thank to Dr. J. Kumar for his valuable suggestions and Dr. K.P. Singh for providing laboratory facilities.

I also thank Mr. R.K. Prasad and Mr. O.P. Malviya for their extensive help throughout this work.

I am indebted to Mr. Mungoøle and Mr. Barthwal for their kind assistance.

My thanks are due to my friends Messers Navin Suyal, Bishwajit Chowdhury, Debjit Biswas, Avimanyu Das, Debasish Bhattacharjee, Shivanand Majagi, Anupam Bagchi, Sanjay Majumdar, Ashoke Kumar, Mukesh Kumar and Anup Verma for their unforgettable cooperation and inspiration.

Finally, I thank Mr. R.N. Srivastava for his excellent typing.

August, 1988

- Sujoy Bhattacharyya

CONTENTS

	Page
LIST OF TABLES	vi
LIST OF FIGURES	viii
ABSTRACT	x
CHAPTER 1 : INTRODUCTION	1
CHAPTER 2 : REPRESENTATION OF PROBLEM	8
CHAPTER 3 : EXPERIMENTAL PROCEDURE	9
3.1: Raw Materials	9
3.2: Coprecipitation	9
3.2.1: Determination of Suitable pH Range	9
3.2.2: Synthesis of the Coprecipitates	10
3.3: Electron Microscopy	11
3.3.1: Sample Preparation	11
3.3.2: Determination of Mean Particle Size and Its Distribution	12
3.4: Differential Thermal and Thermogravimetric Analysis	12
3.4.1: DTA and TGA Procedure	12
3.4.2: DT Study of Fe- and Ba/Fe-complex	13
3.4.3: TG Study of Fe- and Ba/Fe-complex	13
3.5: Ferritization of Coprecipitates	14
3.6: X-ray Powder Diffraction Analysis	14
3.6.1: Qualitative Detection of Different Phases	14
3.6.2: Grain Size Analysis	15
3.7: Ferritization of Pelletized Coprecipitates	16
3.7.1: Sample Preparation	16
3.7.2: Determination of Percent Theoretical Density and Percent True Porosity	16
3.8: Magnetic Measurements	16
3.8.1: Sample Preparation	16
3.8.2: Magnetic Observations	17
CHAPTER 4 : RESULTS	18
4.1: Raw Materials	18
4.2: Coprecipitation	18
4.2.1: Determination of Suitable pH Range	18
4.2.2: Synthesis of Coprecipitate	19
4.3: Determination of Mean Particle Size and Particle Size Distribution by Electron Microscopy	20

	Page
4.4: Differential Thermal and Thermogravimetric Analysis	20
4.4.1: DT Study of Fe- and Ba/Fe-complex	20
4.4.2: TG Study of Fe- and Ba/Fe-complex	21
4.5: Ferritization of Coprecipitates	22
4.6: X-ray Powder Diffraction Analysis	22
4.6.1: Qualitative Detection of Different Phases	22
4.6.2: Grain Size Analysis	23
4.7: Determination of Percent Theoretical Density and Percent True Porosity of the Ferritized Pellets	23
4.8: Magnetic Measurements	23
CHAPTER 5 : DISCUSSION	25
CHAPTER 6 : CONCLUSIONS	31
TABLES	33
FIGURES	55
REFERENCES	73
APPENDIX	75

LIST OF TABLES

Number	Title	Page
1	Magnetic parameters of hexaferrite compounds by different methods of preparation	33
2	Values of pH of mixed chloride solution at different stages of precipitation	34
3	Variation of particle size of coprecipitates with molar dilution of chloride solution	35
4	DT studies of Fe-complex and Ba/Fe-complex	36
5	TG studies of Fe-complex and Ba/Fe-complex	37
6	Standard X-ray powder diffraction data of Fe_2O_3	38
7	Standard X-ray powder diffraction data of $\text{Ba}_3\text{Fe}_2\text{O}_6$	39
8	Standard X-ray powder diffraction data of $\text{BaO} \cdot \text{Fe}_2\text{O}_3$	40
9	Standard X-ray powder diffraction data of $\text{BaO} \cdot 6\text{Fe}_2\text{O}_3$	41
10	X-ray powder diffraction analysis of coprecipitated materials with ferritization temperature of 650°C	43
11	X-ray powder diffraction analysis of coprecipitated materials with ferritization temperature of 750°C	44
12	X-ray powder diffraction analysis of coprecipitated materials with ferritization temperature of 850°C	45
13	X-ray powder diffraction analysis of coprecipitated materials with ferritization temperature of 925°C	46
14	Effect of ferritization temperature on grain size of $\text{BaO} \cdot 6\text{Fe}_2\text{O}_3$	47
15	Effect of pelletization temperature on density and porosity of $\text{BaO} \cdot 6\text{Fe}_2\text{O}_3$	48

Number	Title	Page
16	Effect of ferritization temperature on magnetic property of directly ferritized coprecipitates	49
17	Effect of ferritization temperature on magnetic property of prepressed coprecipitates subsequently ferritized	50
18	Magnetization and demagnetization data of directly ferritized coprecipitated powder	51
19	Magnetization and demagnetization data of prepressed coprecipitates subsequently ferritized	52
20	Magnetization and demagnetization data of prepressed coprecipitates at varying dilutions and ferritization temperature of 925°C	53
21	Magnetization and demagnetization data of coprecipitated powders at varying dilution directly ferritized at 925°C	54

LIST OF FIGURES

Number	Title	Page
1	Phase diagram of BaO- Fe_2O_3 system at $\text{PO}_2 = 1/5$ Atm. in solid phase region and at $\text{PO}_2 = 1$ Atm. in liquid phase region. (1) $2\text{BaO} \cdot \text{Fe}_2\text{O}_3 +$ $\text{BaO} \cdot \text{Fe}_2\text{O}_3$, (2) $\text{BaO} \cdot \text{Fe}_2\text{O}_3 + \text{BaO} \cdot 6\text{Fe}_2\text{O}_3$, (3) $\text{BaO} \cdot 6\text{Fe}_2\text{O}_3 + \text{Fe}_2\text{O}_3$	55
2	The unit cell of $\text{BaO} \cdot 6\text{Fe}_2\text{O}_3$ including ferric ion moment directions	56
3	Domain growth and rotation in ferromagnetic material and associated magnetization curve	57
4	Electron micrographs showing coprecipitated particles of Ba/Fe-complex at varying dilutions (a) Dilution : 0.75(M) Fe (b) Dilution : 0.15(M) Fe (c) Dilution : 0.08(M) Fe (d) Dilution : 0.02(M) Fe	58 58 59 59
5	Histogram showing particle size distribution of coprecipitated Ba/Fe-complex at a dilution of 0.75(M) Fe	60
6	Histogram showing particle size distribution of coprecipitated Ba/Fe-complex at a dilution of 0.08(M) Fe	61
7	DTA and TGA curves of crystalline K_2SO_4 (part- icle size $115 \mu\text{m}$)	62
8	DTA and TGA curves of precipitated BaCO_3	63
9	DTA and TGA curves of precipitated Fe-complex	64
10	DTA and TGA curves of coprecipitated Ba/Fe- complex at dilution of 0.08(M) Fe	65
11	Effect of ferritization temperature on grain size of $\text{BaO} \cdot 6\text{Fe}_2\text{O}_3$	66

Number	Title	Page
12	Effect of pelletization temperature on density and porosity of BaO _{0.6} Fe ₂ O ₃	67
13	Effect of ferritization temperature on magnetic properties of directly ferritized coprecipitates	68
14	Effect of ferritization temperature on magnetic properties of pressed coprecipitates followed by ferritization	69
15	Magnetization curves of coprecipitates ferri- tized by different routes	70
16	Demagnetization curves of the directly ferri- tized coprecipitates	71
17	Demagnetization curves of the prepressed copre- cipitates followed by ferritization	72

CHAPTER - 1

INTRODUCTION

Ceramic magnets are often used in high-frequency applications in which greater electrical resistivity of the ferrimagnetic oxides give them a decisive advantage over metals. Since last 40 years they are being used as circuit elements for radio, television and electronic devices. It has become an essential component as memory units with rapid switching times in digital computer systems. Magnetic ceramics are important as special circuit elements in microwave devices and in devices which rely on their permanent magnetic behaviour. Their cost of production is much cheaper than metallic magnets without any substantial sacrifice of magnetic properties.

Amongst the hexagonal structure ferrimagnetic materials^{1a} which are permanent magnets $\text{BaFe}_{12}\text{O}_{19}$ ($= \text{BaO} \cdot 6\text{Fe}_2\text{O}_3$) is often referred to as barium hexaferrite, or as BaM. It has a magneto-plumbite structure which is represented as $\text{PbFe}_{11}\text{AlO}_{19}$. The same type of structure can be obtained by mixing BaO , SrO or PbO with Fe_2O_3 in suitable proportions. The magnetic oxides having hexagonal structure have been classified as shown in the following table:

Structural formula	Type
MO.6Fe ₂ O ₃	M
2MeO.BaO.6Fe ₂ O ₃	Me ₂ W
2MeO.2BaO.6Fe ₂ O ₃	Me ₂ Y
2MeO.3BaO.12Fe ₂ O ₃	Me ₂ Z
2MeO.2BaO.14Fe ₂ O ₃	Me ₂ X
2MeO.4BaO.18Fe ₂ O ₃	Me ₂ U

where, M = Ba²⁺, Sr²⁺ or Pb²⁺ and

Me = Mn²⁺, Co²⁺, Zn²⁺, Ni²⁺, Mg²⁺ and Fe²⁺.

Numerous compounds have been found in BaO-Fe₂O₃ system.
Figure 1 represents the phase diagram of BaO-Fe₂O₃ system.^{2a}

At room temperature BaO.Fe₂O₃ and BaO.6Fe₂O₃ phases are in solid solution between Fe₂O₃/BaO ratio of 5.0 to 6.0.

The barium ferrite structure^{1b} can be considered as the cubic spinel lattice (designated by S) having the formula Fe₆O₈ separated by hexagonal close-packed section (designated by R) having the formula BaFe₆O₁₁ (Figure 2). The unit cell consists of successive sections of R, S, R*, S*, R, S and so on. S* and R* could be considered as mirror images of S and R-blocks respectively. The total formula for a unit cell is 2(BaFe₁₂O₁₉). The lattice parameter for BaM is a₀ = 5.889 Å, c₀ = 23.18 Å and the theoretical density is 5.28 gm/cc.

The product of magnetic flux density B and associated opposing field H is a useful measure of the performance of a particular hard magnet. It is more commonly known as maximum demagnetization product, $(BH)_{\max}$. It should be substantially large for a permanent magnet. In order to attain a high value of $(BH)_{\max}$, three factors are important^{3a}: (i) a large value of remanence (σ_r), (ii) a large value of coercivity (H_c), and (iii) a rectangular hysteresis loop. The parameters saturation magnetization (σ_s) and coercivity will be briefly discussed in the following sections.

Saturation magnetization^{4a} is the maximum value of magnetization for a ferro- or ferrimagnetic material at the temperature of measurement and it is expressed as emu/gm in cgs unit.

The magnetization of BaM arises from the moment of ferric ions only, each with a spin magnetic moment of $5 \mu_B$ (Bohr Magneton). The magnetization per unit cell is $2(1 + 7 - 2 - 2) \times 5 = 40 \mu_B$.^{1c}

$$\text{Now the unit cell volume} = 694.65 \times 10^{-30} \text{ m}^3 (a_0^2 \cdot \sqrt{3}/2 \cdot C_0)$$

\therefore Saturation Magnetization

$$= 40(\mu_B) \times 1.1653 \times 10^{-29} (\text{Wb-m}) \times \frac{10^{30}}{694.65(\text{m}^3)}$$

$$= 0.671 \text{ Wb/m}^2$$

$$= 0.671 \times 7.96 \times 10^2 \text{ gauss}$$

$$= 534 \text{ gauss}$$

$$= \frac{534}{5.28} \text{ gauss.cm}^3/\text{gm} \text{ (theoretical density} = 5.28 \text{ gm/cm}^3)$$

$$= 101 \text{ gauss.cm}^3/\text{gm} \text{ or, emu/gm}$$

This value is for 0°K .

At 20°C , $\sigma_s = 72$ emu/gm has been reported.⁵

The coercivity^{4b} (i_{c}^H) is defined as the reverse magnetic field required to reduce the magnetic induction of a fully magnetized (i.e., upto saturation magnetization) material to zero. The various parameters controlling coercivity are:

(i) Particle size (with reference to domain theory)^{4c}:

Domains are regions in which magnetic moments of the atoms are aligned in the same direction. The dimension and orientation of domains depend on a balance of the different type of magnetic energies with the interaction energy which causes the spontaneous alignment of atomic moments. Let us consider a single crystal of a ferromagnetic material having only a large domain. This is, however not a desirable situation as the resulting single domain solid with magnetic dipoles at two ends would have a high magnetostatic energy. Splitting of the crystal into several domains can reduce the intensity and extent of the external magnetic field produced by the material and hence the magnetostatic energy. In an unmagnetized sample, the domains themselves are randomly oriented which gives an overall zero magnetic moment as shown in Figure 3. In the magnetization curve (Figure 3), it is shown that saturation is attained by (a) domain growth at initial stage (at lower H), and (b) rotation

of domain moments (at high H). Since domain rotation requires higher energy than domain growth the slope of the M-H curve decreases with increasing H. If a reverse field (-H) is applied, the domain structure will be changed to produce a resultant zero magnetization. So more the magnetostatic energy, more reverse field (H_c^R) has to be applied. Hence in hard magnets like BaM one should always maintain the grain size (often referred to particle size) below the single domain size in order to provide high magnetostatic energy. In BaM, a change in the average grain diameter from 10 to 1 micron increases the coercivity from about 100 to 2000 Oe.⁶

(ii) Magnetocrystalline anisotropy: By this term we mean the dependence of internal energy on the direction of spontaneous magnetization.^{3b} BaM has easy direction of magnetization along its c-axis. As the internal magnetization rotates away by an angle θ from the c-axis, the anisotropy energy increases with an increase of θ , takes its maximum at $\theta = 90^\circ$, and then decreases to its original value at $\theta = 180^\circ$. We can express this energy value as^{2b}:

$$E_a = K_1 \sin^2 \theta + K_2 \sin^4 \theta + K_3 \sin^6 \theta + \dots$$

For BaM compound, K_2 , K_3 are negligible in comparison with K_1 (K is called magnetocrystalline anisotropy constant). Therefore, the above equation is reduced to

$$E_a = K_1 \sin^2 \theta .$$

To rotate the magnetization vector through a more difficult crystal direction requires a maximum reverse field, i.e., the maximum coercivity,

$$H_c = 2K_1/M_s .$$

where, M_s = Saturation magnetization.

So higher the anisotropy energy, higher will be coercivity.

The most effective parameter to increase the coercivity is to maintain the grain size below domain size.

The conventional method for preparing barium ferrite consists of firing a mixture of BaCO_3 and Fe_2O_3 at about 1250°C . The ferritized material is ground to reduce the particle size from multidomain to single domain. Ball milling introduces lattice strains. Observed coercivity values are much less, 1500-3500 Oe than the predicted theoretical value of 6700 Oe.⁵

Several attempts had been made to produce high coercivity hexaferrite compounds. Out of these decomposition method, glass-ceramic method, hot pressing, chemical and electrolytic coprecipitation showed substantially high coercivity (Table 1).

Haneda et al.⁷ prepared BaM by coprecipitation method. They used an alkali mixture of NaOH and Na_2CO_3 to precipitate Ba/Fe-complex from an aqueous solution of FeCl_3 and BaCl_2 mixture taken in suitable proportion. The observed H_c value reported by them is 6000 Oersteds. They took the stoichiometric ratio of Ba/Fe = 1:12, and ferritized at 925°C for 2 hours.

Roos⁸ followed Haneda's route using NaOH solution only as precipitant. He varied the Fe/Ba ratio from 6 to 14. At a ratio of 10.6 he got the highest i_{c}^{H} value of 5500 Oe. The optimum temperature of ferritization was 925°C.

Tanasoiu et al.^{2c} reported a very high i_{c}^{H} value of 6500 Oe obtained for SrM by ordinary dispersion method in ZrO_2 powder or an epoxy resin.

Ghosh⁵ utilized coprecipitation method to prepare BaM. He added $(\text{NH}_4)_2\text{CO}_3$ to a mixture of prerequisite amount of FeCl_3 and BaCl_2 in aqueous solution to coprecipitate Ba/Fe-complex. He tried the coprecipitation with different Ba/Fe-ratios and pH and at a dilution of 0.5(M) Fe of mixed chloride solution. He reported the highest i_{c}^{H} value of 3550 Oe at a Fe/Ba ratio of 10.5. The soaking temperature was 1005°C. The corresponding σ_{max} value was 52.8 emu/gm.

Mallikarjuna⁹ prepared SrM by adding $(\text{NH}_4)_2\text{CO}_3$ solution to aqueous solution of SrCl_2 and FeCl_3 to coprecipitate Sr/Fe-complex. Fe/Sr ratio from 25 to 11 with different pH from 7.2 to 10.0 and dilutions 0.5(M) to 0.02(M) of Fe were maintained. A maximum i_{c}^{H} value of 4.07 KOe with Fe/Sr-ratio of 25.11 at ferritization temperature of 1000°C for 2 hours has been reported. But corresponding σ_{max} -value reported was too low, 28.11 emu/gm. He has also reported an i_{c}^{H} -value of 2.26 KOe and σ_s -value of 56.60 emu/gm with Fe/Sr-ratio of 12 at ferritization temperature of 995°C for 2 hours.

CHAPTER - 2

REPRESENTATION OF PROBLEM

Our aim was to coprecipitate Ba/Fe-complex from their chloride solution at different dilutions and then ferritizing the coprecipitates to get barium hexaferrite after final processing.

Chemical coprecipitation method was chosen due to the advantages like (a) intimate mixing of the starting materials at ionic level, (b) lower ferritization temperature, (c) high coercivity can be achieved as very small grains (below $1 \mu\text{m}$) are developed, (d) absence of lattice strain during milling which incorporates grain growth during ferritization, and (e) high purity can be maintained.

The main objective was to attain a high coercivity along with an appreciable saturation magnetization.

CHAPTER - 3EXPERIMENTAL PROCEDURE3.1: Raw Materials

The following raw materials were used for the preparation of the coprecipitates.

<u>Material</u>	<u>Maker</u>	<u>Quality</u>
Ferric chloride, hexahydrate ($\text{FeCl}_3 \cdot 6\text{H}_2\text{O}$)	S.D. Fine-Chem Pvt. Ltd., Boisar	A.R. Grade
Barium chloride, dihydrate ($\text{BaCl}_2 \cdot 2\text{H}_2\text{O}$)	Glaxo Laboratories (India) Ltd., Bombay	A.R. Grade
Sodium carbonate (Na_2CO_3)	Glaxo Laboratories (India) Ltd., Bombay	A.R. Grade
Sodium hydroxide (NaOH)	Ranbaxy Laboratories Ltd., Punjab	A.R. Grade

3.2: Coprecipitation3.2.1: Determination of Suitable pH Range

Aqueous solutions of FeCl_3 and BaCl_2 were prepared separately in order to know the pH range for the precipitation of the BaCO_3 , Fe-complex and Ba/Fe-complex individually. The alkali mixture of NaOH and Na_2CO_3 was prepared in another beaker.

The alkali solution was slowly added to chloride solutions with vigorous stirring. We used Remi Magnetic Stirrer for

this purpose. The pH before alkali addition, at start of precipitation and end of precipitation were noted by continuous measurement of pH with the help of pH paper.

3.2.2: Synthesis of the Coprecipitate

The pH range was detected by the above experiment for coprecipitation of Ba/Fe-complex. However, we added mixed chloride solution to alkali solution for coprecipitation due to large difference in solubility products of BaCO_3 and Fe(OH)_3 .

A mixture of BaCl_2 and FeCl_3 in solution was taken in a suitable amount. The alkali solution of $\text{NaOH}/\text{Na}_2\text{CO}_3$ was also prepared in required amount following the data supplied by Haneda et al.⁷ which is given below:

H_2O : 400 ml

Amount of NaOH (gm):	10	20	30	40	50	60	70
Amount of Na_2CO_3 (gm):	2.5	5.0	7.5	10.0	12.5	15.0	17.5
Precipitation pH:	7.4	10.4	11.8	12.0	>13.2	>13.2	>13.2

We selected the composition of 50 gm NaOH and 12.5 gm Na_2CO_3 in 400 ml. water as mentioned by Haneda et al.⁷ The amount of FeCl_3 and BaCl_2 solution was so taken that Fe/Ba-ratio remained 11:1 in BaM.

The mixed chloride solution was slowly added to the alkali mixture with vigorous stirring. The coprecipitation was

carried out for 5 minutes at room temperature.

Without holding the solution the coprecipitated material was filtered through Whatman-40 filter paper, and thoroughly washed with water to make it alkali free.

The coprecipitates were then collected from the filter paper and dried in electric oven at 80°C for one day. The granulated coprecipitates were then ground to powder by agate mortar and pestle.

3.3: Electron Microscopy

3.3.1: Sample Preparation

Sample preparation was done following the technique described by Allen¹⁰ as described below.

A solution of 2% (w/v) polyvinyl formal (formvar) in chloroform was prepared and transferred to a 50 ml beaker. Clean glass slide was dipped into that solution and instantaneously withdrawn. The polymer film was allowed to dry in a desiccator for one hour. The film was separated from the slide by scratching the edges by a scalpel and dipping the slide in distilled water slowly from one edge of the slide. The film finally floated on water. A 200-mesh copper grid (3 mm diameter) was placed on that film. The grid was then 'fished' quickly on a clean glass slide so that the grid rested on the side and the film on grid. The slide was then dried in a desiccator for one day.

Coprecipitation was done at five different dilutions of mixed chloride solution as described in 3.2.2. After the coprecipitation was over the solution was about ten times diluted with distilled water. The whole solution was then again stirred by magnetic stirrer. A little amount of the solution was withdrawn by a hypodermic syringe and a droplet was pushed to the film coated grid from the syringe. The sample was then dried in a desiccator for one day. It was then studied under electron microscope using Philips EM 301 transmission electron microscope.

3.3.2: Determination of Mean Particle Size and Its Distribution¹¹

Mean particle size was calculated from the microphotographs.

$$\text{Mean particle size} = \frac{\sum n_i d_i}{\sum n_i}$$

where, n_i = Number of particles with average size d_i .

Distribution was also found out by counting the particles.

3.4: Differential Thermal and Thermogravimetric Analysis

3.4.1: DTA and TGA Procedure

DT and TG studies of precipitated BaCO_3 , Fe-complex and coprecipitated Ba/Fe-complex was done by Linseis GMBH D8672 SELB DT/TG apparatus. The dried coprecipitated powders were weighed and set for the experiment. The type of reactions (endo- or

exothermic) and reaction temperatures were plotted by DT curves. And the weight loss was plotted by the TG curves.

The peak areas were measured by planimeter. Crystals of K_2SO_4 (particle size 115 μm) which has a reversible phase transformation at $565^{\circ}C$ was taken as standard to measure the heat of different reactions.¹² The heat of transformation was calculated from the peak area. This value was compared with the peak areas obtained from the precipitated samples.

The heating rate for DT and TG analysis was maintained at $5^{\circ}C/min.$

3.4.2: DT Study of Fe- and Ba/Fe-complex

The heat of dehydroxilation and ferritization reaction of the Ba/Fe-complex was computed as described in 3.4.1. Also the heat of dehydroxilation of Fe-complex was computed in the same way.

3.4.3: TG Study of Fe- and Ba/Fe-complex

The cumulative weight loss was calculated from the TG curves. Assuming the whole loss of weight is due to dehydroxilation only, we estimated a chemical formula of the Fe-complex and Ba/Fe-complex. From standard data for heat of evaporation of water, a comparison was made with the heat of dehydroxilation values obtained from the precipitates.

3.5: Ferritization of Coprecipitates

Two sets of experiments were done. In one set coprecipitate was obtained from a 0.15(M) of FeCl_3 solution. It was then ferritized to different temperatures. In another set coprecipitation was done out of different dilutions and ferritization at a fixed temperature of 925°C . Electrically heated tubular resistance furnace was used. The Pt/Pt + 10% Rh thermocouple was used for temperature measurement.

A longitudinal temperature profile was taken before ferritization to find the constant temperature zone of the furnace. Isothermal heating was done. The required temperature was obtained first and the sample was then quickly introduced to the constant temperature zone. Ferritization was done for 2 hours in air followed by normal cooling.

3.6: X-ray Powder Diffraction Analysis

3.6.1: Qualitative Detection of Different Phases

For identification of different phases present in the samples ferritized at different temperature X-ray powder diffraction pattern was taken using Philips Iso-Debyeflex 2002D diffractometer. Two sets of experiments were done. One for the samples obtained from the mixed chloride solution of dilution 0.15(M) Fe and different ferritization temperatures. Another obtained from different dilution of mixed chloride solutions and ferritization temperature of 925°C .

All X-ray diffractograms were taken using CrK_α radiation (wavelength = 2.291002 \AA) at a scanning speed of $3^\circ/\text{minute}$ in 2θ , tube voltage 40 KV and time constant 10 seconds.

3.6.2: Grain Size Analysis

From the same diffraction patterns grain size was determined using line broadening method as described by Cullity.¹³ The grain size (\AA) is given by:

$$t = \frac{0.9 \lambda}{B \cos\theta}$$

where, $B = (B_M^2 - B_S^2)^{1/2}$

λ = Wavelength of X-ray radiation, \AA

B_S, B_M = Band width at half of the maximum intensity of a peak for the standard sample and the unknown sample respectively, in radiation

θ = Bragg angle of diffraction at maximum intensity.

We used NaCl as standard sample. The half-intensity band width for NaCl was taken at $2\theta = 48.15^\circ$, and that for ferritized samples at $2\theta = 48.67^\circ$ because those were the closest matching peaks. This calculation was based on the grain size of the barium hexaferrite phase. In another set of estimation BaM prepared at 1200°C for 6 hours was used as standard material.

3.7: Ferritization of Pelletized Coprecipitates

3.7.1: Sample Preparation

Coprecipitates obtained from a mixed chloride solution of dilution 0.15 (M) Fe were pressed to pellets at pressures of 1.80 Kg/mm² by hydraulic press. The pellets were then sintered to ferritization at 850°, 925°, 1000°, 1100° and 1200°C. Geometrical measurements and weights of the ferritized pellets were noted.

3.7.2: Determination of Percent Theoretical Density and Percent True Porosity

$$\text{Percent theoretical density} = \frac{D_B}{D_T} \times 100$$

$$\text{and, Percent true porosity} = (1 - \frac{D_B}{D_T}) \times 100$$

where, D_B = Bulk density of the sample
 $= \frac{\text{Sample weight (gm)}}{\text{Sample volume (cc)}}$,

D_T = Theoretical density
 $= 5.28 \text{ gm/cc.}$

3.8: Magnetic Measurements

3.8.1: Sample Preparation

Two sets of samples were prepared from the coprecipitates: (i) coprecipitates directly ferritized and then passed to small cylindrical shape (3 mm diameter and about equal

height) and (ii) coprecipitates prepressed followed by ferritization.

In the first set 2% (w/v) polyvinyl alcohol (PVA) was added to the ferritized powder to incorporate green strength of the samples. The weight of PVA was compensated for exact weight of the samples.

Each set was again subdivided into two subsets:

(a) constant ferritization temperature of 925°C and different dilutions of 0.75(M), 0.25(M), 0.15(M), 0.08(M) and 0.02(M) and (ii) constant dilution of 0.15(M) and different ferritization temperatures of 650° , 750° , 850° , 925° , 1000° , 1050° , 1100° , 1150° and 1200°C .

3.8.2: Magnetic Observation

Parallel field vibrating sample magnetometer Model 150A was used to measure coercivity, saturation magnetization and remanence. A maximum field of 9 KOe was applied.

CHAPTER - 4RESULTS4.1: Raw Materials

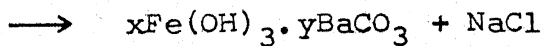
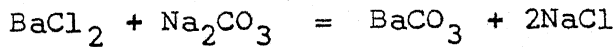
$\text{FeCl}_3 \cdot 6\text{H}_2\text{O}$ crystals were highly hygroscopic. Therefore concentration of iron in ferric chloride solution was determined volumetrically as described in Appendix. Concentration of Fe in FeCl_3 -solution was found to be 0.0060 gm/ml.

4.2: Coprecipitation4.2.1: Determination of Suitable pH Range

Mixed alkali solution was added to chloride solution slowly as described in 3.2.1.

BaCO_3 precipitate was not stable in acidic region (at a pH below 7).

Deep brown precipitation occurred as soon as the mixed chloride solution was added to the alkali mixture. The probable chemical reactions are as follows:



The pH at different precipitation stages is shown in Table 2.

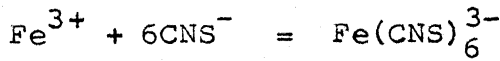
4.2.2: Synthesis of Coprecipitate

Coprecipitation was done in such a way so that after the precipitation was over the pH of solution remained greater than 12.

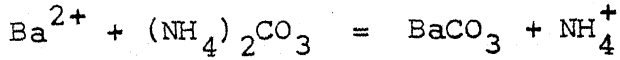
Five different mixed chloride solutions of dilution 0.75 (M), 0.25 (M), 0.15 (M), 0.08 (M) and 0.02 (M) of Fe were taken.

To ensure that precipitation was over the absence of Ba^{2+} -ion and Fe^{3+} -ion in the filtrate was tested qualitatively.¹⁴

The presence of Fe^{3+} -ion was detected by adding excess potassium thiocyanate solution to the filtrate. A dark, reddish-brown precipitate confirms the presence of Fe^{3+} ion.



The presence of Ba^{2+} -ion was confirmed by a white precipitation obtained by adding $(\text{NH}_4)_2\text{CO}_3$ to the filtrate.



The pH of the solution was always checked by pH paper so that it remained above 12. After the precipitation was over the precipitate was made alkali free by pouring water through the filter paper thoroughly. This operation was carried out till the filtrate showed a neutral pH of 7.

4.3: Determination of Mean Particle Size and Particle Size Distribution by Electron Microscopy

Figure 4 shows the electron micrograph of coprecipitated particles at dilutions 0.75(M), 0.15(M), 0.08(M) and 0.02(M) of Fe. For dilutions 0.75(M) and 0.08(M) the shape of particles were spherical. So we directly counted the number of particles having an average diameter. For dilutions 0.15(M) and 0.02(M) we got non spherical particles. We measured the maximum length and minimum breadth of each particle and took the average to calculate the mean diameter. Table 3 shows the variation of particle size with dilution of chloride solution. Figures 5 and 6 represent the histogram of particle size distribution. Particle size decreased with increasing dilution of chloride solution.

4.4: Differential Thermal and Thermogravimetric Analysis

4.4.1: DT Study of Fe- and Ba/Fe-complex

Figures 8, 9 and 10 represent DT and TG curves of precipitated BaCO_3 , Fe- and Ba/Fe-complexes respectively. The result of DT analysis is computed in Table 4. A DT/TG analysis was also done for the K_2SO_4 crystals having a reversible transformation characteristics taken as a standard material (Figure 7) for determination of heat of hydroxitation and ferritization reactions.

Figure 7 shows an endothermic peak at 565°C due to the crystal structure transformation of K_2SO_4 .

Figure 8 shows an endothermic peak at 790°C possibly due to the rearrangement and transition into different crystal structure of BaCO_3 .⁵

Figure 9 shows a small endothermic peak at 250°C which is supposed to be due to dehydroxilation of the Fe-complex.

Figure 10 shows an endothermic peak at 120°C which is due to the dehydroxilation reaction of the Ba/Fe-complex. The exothermic peak at 670°C confirms the ferritization reaction.⁸

The heat of dehydroxilation and ferritization reactions are tabulated in Table 4.

4.4.2: TG Study of Fe- and Ba/Fe-complex

The cumulative percent weight loss is computed in Table 5.

Precipitated BaCO_3 did not show any weight loss (Figure 8). But the Fe-complex (Figure 9) and Ba/Fe-complex (Figure 10) showed appreciable weight loss which is supposed to be due to loss of water during dehydroxilation.

The chemical formula had been proposed for the Fe-complex and Ba/Fe-complexes obtained from three different dilutions 0.75 (M), 0.15 (M) and 0.08 (M) of mixed chloride solutions. As we took the $\text{FeCl}_3 \cdot 6\text{H}_2\text{O}$ and $\text{BaCl}_2 \cdot 2\text{H}_2\text{O}$ in aqueous solution so that the Fe/Ba ratio remains 11:1 in BaM, the chemical formula of the coprecipitated Ba/Fe-complex is assumed to be $5.5\text{Fe}_2\text{O}_3 \cdot \text{BaCO}_3 \cdot n\text{H}_2\text{O}$. The value of n varied with dilution (Table 5). But we did not find any significant correlation

between n-value and dilution. For the Fe-complex the formula was assumed to be $\text{Fe}_2\text{O}_3 \cdot m\text{H}_2\text{O}$, where m estimated from weight loss was 2.48. The comparison between heat of dehydroxilation value obtained from DTA and that obtained from standard data of heat of evaporation of water (10.12 Kcal/mole at 298°K , 1 atm.) and TG analysis is tabulated in Table 5.

4.5: Ferritization of Coprecipitates

Coprecipitates were obtained from the mixed chloride solution of dilution 0.15(M) Fe. The dried coprecipitates were ferritized at 650° , 750° , 850° , 925° , 1000° , 1050° , 1100° , 1150° and 1200°C for 2 hours.

In another set coprecipitation was done out of mixed chloride solutions of dilution 0.75(M), 0.25(M), 0.15(M), 0.08(M) and 0.02(M) of Fe. The dried coprecipitates were ferritized at 925°C for 2 hours.

The temperature variation inside the furnace was noted to be $\pm 5^\circ\text{C}$.

4.6: X-ray Powder Diffraction Analysis

4.6.1: Qualitative Detection of Different Phases

The result of X-ray analysis is given in Tables 10-13. Above a ferritization temperature of 925°C only $\text{BaO} \cdot 6\text{Fe}_2\text{O}_3$ was present. For the sample ferritized at 650°C , peaks of $\text{BaO} \cdot \text{Fe}_2\text{O}_3$ and Fe_2O_3 were observed. For the sample ferritized at 750°C a peak was observed at $2\theta = 36.58$ ($I/I_0 = 100$) which resembles

the $\text{Ba}_3\text{Fe}_2\text{O}_6$ (with $I/I_0 = 3$ in reference) phase, but we nevertheless marked it to be undetected due to the large difference in the I/I_0 ratio. We shall discuss about it in Chapter 5.

Peaks of Fe_2O_3 were observed in the sample ferritized at 850° . At 925°C all the peaks observed are due to $\text{BaO} \cdot 6\text{Fe}_2\text{O}_3$ only.

Standard powder diffraction data¹⁵ are represented in Tables 6-9. Presence of different phases in our sample was identified from these standard data available.

4.6.2: Grain Size Analysis

Grain size analysis was done by line broadening method which has been already described in 3.6.2. Grain size of the coprecipitates ferritized at 650° , 750° , 850° , 925° , 1000° , 1050° , 1100° , 1150° and 1200°C were measured and the results are tabulated in Table 14. Figure 11 shows the curve for grain size as a function of ferritization temperature. Grain size increases sharply after 1000°C .

4.7: Determination of Percent Theoretical Density and Percent True Porosity of the Ferritized Pellets

With the increase in ferritization temperature the theoretical density increased and porosity decreased. This effect was quite sharp above 950°C (Figure 12). The experimental data are tabulated in Table 15.

4.8: Magnetic Measurements

Coercivity (H_c^i), saturation magnetization (σ_s) and remanence (σ_r) were measured as described in 3.8.1 and 3.8.2.

The effect of ferritization temperature on magnetic properties are tabulated in Tables 16 and 17, and diagrammatically represented in Figures 13 and 14.

For a dilution of 0.15(M) Fe, the σ_s increased from 20.82 emu/gm to 55.42 emu/gm for ferritization temperature of 650°C to 1200°C respectively (Table 16). Above 1000°C , a step increase in σ_s was observed. The σ_r also follow the same characteristics. i_c^H increases upto 1050°C and after that it falls remarkably. For the samples obtained from different dilutions and same ferritization temperature no significant variation in magnetic properties was observed. At a dilution of 0.75(M) and ferritization temperature 925°C a very high σ_s value of 75 emu/gm was observed.

Tables 18-21 represent the magnetization and demagnetization data of the ferritized samples. The magnetic properties obtained from this table has been already represented in Tables 16 and 17.

Figure 15 represents the magnetization curves of the coprecipitates ferritized by different routes. Both of the curves represent the samples ferritized at 1050°C . For the sample obtained from the directly ferritized coprecipitate a higher value of σ_s was observed.

Figures 16 and 17 represent the demagnetization curves of the coprecipitates ferritized by different routes and different temperatures. In both of the cases a highest i_c^H value of 4.15 KOe has been observed for the ferritization temperature of 1050°C .

CHAPTER - 5DISCUSSIONS

In 4.2.1 the determination of the suitable pH range for the coprecipitation of Ba/Fe-complex has been discussed. To ensure precipitation of BaCO_3 and Fe-complex simultaneously mixed chloride solution was added to the alkali solution. This is due to the fact that solubility products of BaCO_3 and Fe(OH)_3 are 7×10^{-9} (16°C) and 1.1×10^{-36} (18°C)¹⁶ respectively. Had the method been followed as described in 3.2.1 Fe(OH)_3 would have been precipitated before BaCO_3 because of lower solubility product value of the former. And it would not be a case of coprecipitation.

The coprecipitate was synthesised as described in 4.2.2.

The precipitate did not dissolve above pH of 10. However a pH greater than 12 was always maintained for stability of BaCO_3 as reported by Haneda et al.⁷

The DT and TG curves (Figure 10) of the Ba/Fe-complex are similar to those reported by Roos.⁸ He had reported the endothermic peak at 130°C and exothermic one at 760°C . We obtained the peaks at 120°C and 670°C respectively. Roos used a dilution of 0.75(M) of chloride solution and we used a dilution of 0.08(M). In our case the particle size of the coprecipitate is expected to be smaller than that obtained by Roos (Table 3).

An increase in peak temperature with increase in particle size for ferritization reaction has been observed from DTA (Table 4). It is most probably due to the fact that for smaller particles rate of reaction is faster because more surface area is available. In a steady rate of heating therefore, coarser particles will react more slowly than the finer one. This effect would be reflected in DT curve by a shift of peak temperature to a higher value.

Roos⁸ reported a net weight loss of about 20% from TGA for Ba/Fe-complex. The DT curve reported by him behaved in similar manner as for $\text{Ba}(\text{OH})_2 \cdot \text{H}_2\text{O}$. He took a Fe/Ba-ratio of 10.6. On that basis the loss of weight is supposed to be about 24%. The 20% weight loss reported by Roos proved that $\text{Fe}(\text{OH})_3$ lost less than theoretical amount of water. In our experimental sample (Figure 10) the weight loss was 15.85%. It means a less amount of water is associated with the Ba/Fe-complex in this case than it was supposed to be with $\text{Fe}(\text{OH})_3$. This lower value is a good agreement with the similarly reduced value reported by Roos.

The chemical formulae of the Ba/Fe-complex based on TGA (Table 5) were proposed. No significant relationship of amount of associated water with dilution of mixed chloride solutions has been observed.

We have also tried to calculate the heat of dehydroxylation (ΔH_D) obtained from DTA and TGA both as described in 4.4.1 and 4.4.2 respectively. The results in Table 5 show a

discrepancy in the values of ΔH_D obtained by DTA as compared to those by TGA. The ΔH_D obtained from DTA must be greater than that obtained from TGA because structurally bonded water would require more energy for its dissociation as compared to the evaporation of loosely associated water. As the ΔH_D value obtained from DTA is lower than that obtained from TGA, the results appear to be anomalous because there must be some combined water associated with the coprecipitates.

Ghosh⁵ has reported an endothermic peak at 860°C in DTA for precipitated BaCO₃ with no corresponding weight loss in TGA. In our sample the same peak was observed at 790°C without any weight loss.

If we express the particle size of BaCO₃ as a function of dilution of mixed chloride solution, it would be observed that the particle size of BaCO₃ did not exceed 168 Å for a dilution of 0.5(M) in Ghosh's experiment whereas for same dilution it was greater than 400 Å (Table 3) in our sample.

It was observed by Natarajan et al.¹² that crystal structure transformation temperature decreases with increase in particle size while heating. The same phenomena was reflected to our experimental results for BaCO₃ which undergoes a structural transformation.

From X-ray powder diffraction analysis, we find a peak (Table 11) at $2\theta = 36.58^\circ$ ($I/I_0 = 100$) which corresponds to the peak for Ba₃Fe₂O₆ ($I/I_0 = 3$) as shown in Table 7 in standard data. This is a spurious result however because other higher

intensity peaks ($I/I_0 > 3$) for this phase were missing in that diffractogram. Two peaks of $\text{BaO} \cdot \text{Fe}_2\text{O}_3$ were observed at $2\theta = 87.20^\circ$ and $2\theta = 89.58^\circ$ for the sample ferritized at 650°C as shown in Table 10. At 750°C reacted sample two peaks at $2\theta = 104.11^\circ$ ($I/I_0 = 36$) and $2\theta = 111.15^\circ$ ($I/I_0 = 34$) remained unidentified (Table 11). Those data were compared with standard data noted in this report and also with the data of $\text{BaO} \cdot \frac{1}{2}\text{Fe}_2\text{O}_3$ as reported by Ghosh.⁵ At 850°C reacted sample (Table 12) two peaks of Fe_2O_3 at $2\theta = 70.00^\circ$ ($I/I_0 = 79$) and $2\theta = 86.88^\circ$ ($I/I_0 = 54$) were observed in the diffractogram. The presence of $\text{BaO} \cdot \text{Fe}_2\text{O}_3$ phases are perhaps due to incomplete ferritization at 650°C . The presence of Fe_2O_3 is probably due to the local inhomogeneity in the coprecipitates which had left some Fe_2O_3 unreacted with the Ba-complex. Above 925°C (Table 13), only peaks of $\text{BaO} \cdot 6\text{Fe}_2\text{O}_3$ were observed. It appears that 925°C is sufficient temperature for complete ferritization. This fact agrees with the $\text{BaO}-\text{Fe}_2\text{O}_3$ phase diagram (Figure 1) where at $\text{Fe}_2\text{O}_3/\text{BaO} = 5.5$ a single phase solid solution region of $\text{BaO} \cdot 6\text{Fe}_2\text{O}_3$ is seen at room temperature.

The grain size of hexaferrite increased with ferritization temperature (Table 14). Figure 11 shows the grain size vs. ferritization curve which is in good agreement with the results obtained by Haneda et al.⁷

There is a step increase in grain size above the ferritization temperature of 1000°C . Also in Figure 12 we see that there is a step increase in percent theoretical density and

decrease in true porosity above 950°C. Figures 13 and 14 show a reduction of i^H_C above 1050°C of ferritization temperature.

From the discussions in the above paragraph it is evident that densification starts to occur from 950°C accompanied by grain growth. The reduction in coercivity above 1050°C proves that appreciable grain growth had been taken place which is responsible for domain nucleation inside an individual grain. The reduction in i^H_C has a temperature lag of 50°C behind grain growth.

Haneda et al.⁷ have observed a reduction of coercivity above 950°C of ferritization temperature. Saturation magnetization attained a maximum value at that temperature and remained almost constant. We observed the same phenomena (Figures 13 and 14) but at a different ferritization temperature of 1050°C. Tables 16 and 17 show that i^H_C increases to maximum value of 4.15 KOe from a very low value upto 1050°C. This is because at low temperature sufficient BaM phase did not develop.

The maximum i^H_C obtained by Haneda et al.⁷ and Roos⁸ were 6.0 KOe and 5.5 KOe respectively at ferritization temperature of 925°C.

A σ_s value of 72 emu/gm has been reported by Tauber et al.^{2d} Still a higher value of 75 emu/gm has been reported in our sample obtained from a dilution of 0.75(M) and ferritized at 925°C (Table 21).

From Tables 16 and 17 a great mismatch in σ_s values were observed between the sample obtained from a dilution of 0.15(M)

and those obtained from dilutions of 0.75(M), 0.25(M), 0.08(M) and 0.02(M), all of them ferritized at 925°C. The σ_s value in the preceding one was extremely low (Below 37 emu/gm) as compared to other four values (above 50 emu/gm). No satisfactory explanation could be made for this anomalous observation.

CHAPTER - 6CONCLUSIONS

- (1) Coprecipitation of Ba/Fe-complex can be done by adding a solution of BaCl_2 and FeCl_3 to an alkali solution of NaOH and Na_2CO_3 .
- (2) The pH at the end of coprecipitation was above 12.
- (3) Mean particle size of the coprecipitated material decreased with increasing dilution.
- (4) The precipitated Fe-complex decomposed at 250°C to form Fe_2O_3 which reacted with Ba-complex to form barium hexaferrite at $\sim 700^\circ\text{C}$.
- (5) No significant effect of dilution of mixed chloride solution on estimated formula of Ba/Fe-complex was observed.
- (6) The ferritization reaction temperature and heat of ferritization decreased with increase in dilution (decreasing particle size).
- (7) Formation of barium hexaferrite phase was complete at 925°C .
- (8) At ferritization temperature lower than 925°C , $\text{BaO} \cdot \text{Fe}_2\text{O}_3$ and Fe_2O_3 phases were present.
- (9) The grain size of the BaM increased with ferritization temperature. It was $\sim 0.6 \mu\text{m}$ at 1000°C .
- (10) Percent theoretical density increased and true porosity decreased with increasing ferritization temperature. A sharp change of these two properties were observed above 950°C .

(11) Samples ferritized at 1050°C showed a maximum coercivity of 4.15 KOe obtained from a dilution of 0.15(M) with a corresponding saturation magnetization of 52 emu/gm.

(12) The coercivity obtained by us was about 62% of theoretical value (6.7 KOe). The following experiments could be carried out to improve it:

- (a) An optimization of magnetic properties could be done by ferritizing the coprecipitates at 950° , 1000° and 1050°C obtained from the dilutions of 0.75(M), 0.25(M), 0.08(M) and 0.02(M).
- (b) Only NaOH solution could be tried instead of NaOH/ Na_2CO_3 mixture for coprecipitation.
- (c) Different Ba/Fe-ratio could be tried.
- (d) Different pH could be tried.

Table 1: Magnetic parameters of hexaferrite compounds by different methods of preparation.

Compound	D_c^* (m)	$\sigma_w^{\#}$ (erg/cm ²) (KOe)	$M_{HC}^{\#}$ (emu/g)	σ_s (emu/g)	Preparation method	Remarks
Ba _{0.6} Fe ₂ O ₃	0.90	9.0	6.0	63.4	Coprecipitation from glass	$H_A = 17.2$ KOe, $\bar{D} = 4600\text{\AA}$
			6.4	70.7	Coprecipitation and leached with HCl	$\bar{D} = 1000\text{\AA}$
			5.35	60.3	Coprecipitation	$P = 0.3$, $D/t = 15$,
			2.8	4.80	Coprecipitation as oxalate	$\bar{D} = 800 - 1500\text{\AA}$
			6.50	63.5	Ball milled and annealed	$P = 0.025$
						$\bar{D} = 800 - 1000\text{\AA}$
Sr _{0.6} Fe ₂ O ₃	0.94	8.0	5.75	55.0	Coprecipitation	$P = 0.30$
Pb _{0.6} Fe ₂ O ₃	0.70	4.82				

* Approximately estimated value as a sphere, # By domain observation
 D_c : Critical dia. of single domain particle, σ_w : Domain wall energy per unit area,

$M_{HC}^{\#}$: Coercivity, σ_s : Saturation magnetization, \bar{D} : Average diameter, P : Packing factor,
 D/t : Dia. to thickness ratio.

(Ref. Kojima, H., "Fundamental properties of hexagonal ferrites with magnetoplumbite
structure", in "Ferromagnetic materials", Vol. 3", Ed. Wohlfarth, E.P., North-Holland,
1982, p. 335).

Table 2: Values of pH of mixed chloride solutions at different stages of precipitation.

Precipitation stage	BaCl ₂ solution * (pH)	FeCl ₃ solution * (pH)	BaCl ₂ / FeCl ₃ solution * (pH)
Before alkali addition	3 - 4	2 - 3	1 - 2
At start of precipitation	6	4	4
At end of precipitation	10	8	10

* with gradual addition of NaOH/Na₂CO₃ mixture

2 3

Table 3: Variation of particle size of coprecipitates with molar dilution of chloride solution.

Dilution (mole Fe)	Mean particle size (Å)
0.75	573
0.15	408
0.08	284
0.02	121

Table 4: DT study of Fe - complex and Ba/Fe - complex.

Dilution (mole Fe)	Dehydroxilation				Ferritization			
	ΔH (kcal/ mole)	Tstart (°C)	Tpeak (°C)	Tend (°C)	ΔH (kcal/ mole)	Tstart (°C)	Tpeak (°C)	Tend (°C)
0.75 (Ba/Fe)	125.8	40	110	320	14.56	590	690	700
0.15 (Ba/Fe)	104.8	40	130	220	-	-	-	-
0.08 (Ba/Fe)	89.83	40	120	240	12.3	650	670	690
0.75 (Fe)	0.938	200	250	300	-	-	-	-

Table 5: TG study of Fe-complex and Ba/Fe-complex

Dilution (mole Fe) (Ba/Fe)	Cumulative weight loss (%)	Upto (°C)	Cumulative weight loss (%)	Upto (°C)	Heat of dehydroxilation, ΔH , (Kcal/mole)	Proposed formula
		TGA		DTA		
0.75 (Ba/Fe)	15.16	320	16.75	830	121.44	125.792
0.15 (Ba/Fe)	15.23	220	19.05	720	141.68	104.813
0.08 (Ba/Fe)	11.58	240	15.85	770	111.32	89.835
0.75 (Fe)	18.40	300	21.83	800	25.10	0.938
						$\text{Fe}_2\text{O}_3 \cdot 2 \cdot 48\text{H}_2\text{O}$

Table 6: Standard powder diffraction data of Fe O (Ref. 15a)

2 3

d (Å)	I/I ₀	2θ (degree)	hkl
6.470	4	20.40	011
3.240	20	41.41	400
3.150	4	42.65	031
2.981	35	45.20	411
2.728	100	49.66	420
2.548	20	53.43	040
2.458	30	55.55	511
2.243	20	61.42	512
2.176	14	63.53	521
1.997	20	70.00	440
1.983	20	70.41	620
1.735	25	82.60	720
1.666	25	86.88	721
1.520	35	97.81	552
1.469	30	102.5	732
1.383	30	111.8	921

Table 7: Standard powder diffraction data of Ba Fe O (Ref. 15b)

3 2 6

d (Å)	I/I ₀	2θ (degree)	hkl
5.040	2	26.27	311
4.470	2	29.70	320
4.180	20	31.81	400
3.830	10	34.81	331
3.650	3	36.58	421
3.420	1	39.14	422
3.220	15	41.68	511
3.100	5	43.37	520
3.050	2	44.12	521
2.958	100	45.57	440
2.416	18	56.61	444
2.092	35	66.40	800
1.708	30	84.24	844

Table 8: Standard powder diffraction data of BaO.Fe O (Ref. 15c)

2 3

d (Å)	I/I ₀	2θ (degree)	hkl
7.730	10	17.03	111
4.770	8	27.79	400
4.690	12	28.27	210
4.430	6	29.97	111
3.160	65	42.51	402
3.130	100	42.94	212
2.736	40	49.50	610
2.688	20	50.45	020
2.589	4	52.52	701
2.547	4	53.45	121
2.111	16	65.73	004
2.047	18	68.06	422
1.671	16	86.55	614
1.661	10	87.20	024
1.626	10	89.58	232
1.562	8	94.34	630

Table 9: Standard powder diffraction data of Ba_{0.6}Fe_{0.4}O₃ (Ref. 15d)
2 3

d (Å)	I/I ₀	2θ (degree)	hkl
4.980	12	26.60	101
4.670	21	28.40	102
3.870	11	34.43	006
3.830	5	34.81	104
3.080	9	43.67	106
2.950	56	45.70	110
2.900	17	46.53	008
2.855	11	47.31	112
2.780	100	48.67	107
2.630	88	51.64	114
2.550	10	53.39	200
2.536	7	53.71	201
2.520	7	54.07	108
2.420	45	56.50	203
2.343	5	58.54	116
2.236	31	61.63	205
2.130	25	65.07	206
1.949	7	71.99	1011
1.823	4	77.86	1110
1.813	9	78.37	201
1.716	4	83.76	2010
1.701	8	84.86	300

(continued to p. 42)

(continuation from page 41)

Table 9: Standard powder diffraction data of Ba_{0.6}Fe_{0.4}O (Ref. 15d)

2 3

d (Å)	I/I ₀	2θ (degree)	hkl
1.667	43	86.81	217
1.657	7	87.47	0014
1.632	25	89.16	304
1.625	46	89.65	2011
1.616	6	90.28	1112
1.606	8	91.00	218
1.541	5	96.03	2012
1.473	37	102.09	220
1.423	6	107.22	2111
1.390	14	110.99	2014
1.318	1	120.71	1017
1.313	11	121.48	228
1.302	22	123.24	317
1.301	5	123.40	1116

Table 10: X-ray powder diffraction analysis of coprecipitate

Ferritization temperature : 650°C

d (Å)	I/I ₀	2θ (degree)	hkl	Remarks
2.950	69	45.70	110	BaFe O 12 19
2.780	86	48.67	107	"
2.630	97	51.64	114	"
2.420	66	56.50	203	"
2.236	60	61.63	205	"
1.661	63	87.20	024	BaO.Fe O 2 3
1.626	54	89.58	232	"
1.469	100	102.48	732	Fe O 2 3

Table 11: X-ray powder diffraction analysis of coprecipitate

○
Ferritization temperature : 750 °C

d (Å)	I/I ○	2θ (degree)	hkl	Remarks
3.650	100	36.58	—	undetected
2.950	58	45.70	110	BaFe O 12 19
2.780	64	48.67	107	"
2.630	73	51.64	114	"
2.520	38	54.07	108	"
2.236	30	61.03	205	"
2.130	28	65.07	206	"
1.667	41	86.81	217	"
1.625	51	89.65	2011	"
1.473	61	102.1	220	"
—	36	104.1	—	undetected
—	34	111.1	—	"

Table 12: X-ray powder diffraction analysis of coprecipitate

Ferritization temperature : 850 °C

d (Å)	I/I ₀	2θ (degree)	hkl	Remarks
2.950	51	45.70	110	BaFe O 12 19
2.780	95	48.67	107	"
2.630	97	51.64	114	"
2.420	54	56.50	203	"
2.236	62	61.63	205	"
1.997	79	70.00	440	Fe O 2 3
1.666	54	86.88	721	Fe O 2 3
1.625	85	89.65	2011	BaFe O 12 19
1.473	100	102.1	220	"

Table 13: X-ray powder diffraction analysis of coprecipitate

Ferritization temperature : 925 °C

d (Å)	I/I ₀	θ (degree)	hkl	Remarks
2.950	57	45.70	110	BaFe O 12.19
2.780	100	48.67	107	"
2.630	83	51.64	114	"
2.420	56	56.50	203	"
2.236	43	61.63	205	"
2.130	44	65.07	206	"
1.667	50	86.81	217	"
1.625	76	89.65	201I	"
1.473	67	102.1	220	"

Table 14: Effect of ferritization temperature on grain size of $\text{BaO} \cdot 6\text{Fe}_2\text{O}_3$.

Dilution (mole Fe)	Ferritization temperature (°C)	Grain Size (μm)	
		NaCl standard	$\text{BaO} \cdot 6\text{Fe}_2\text{O}_3$ standard
0.15	650	0.22	0.23
"	750	0.29	0.37
"	850	0.46	0.39
"	925	0.48	0.41
"	1000	0.66	0.60
"	1050	0.66	0.60
"	1100	0.74	0.70
"	1150	0.86	0.85
"	1200	1.50	-
0.08	925	0.55	0.49
0.02	925	0.74	0.70

Table 15: Effect of pelletization temperature on density and porosity of $\text{BaO} \cdot 6\text{Fe}_2\text{O}_3$.

Ferritization temperature (°C)	Theoretical density (%)	True porosity (%)
850	78	22
925	79	21
1000	93	07
1100	95	05
1200	98	02

Table 16: Effect of ferritization temperature on magnetic property.

Directly ferritized coprecipitates

Dilution (mol Fe)	Ferritization temperature	σ_s (emu/g)	σ_r (emu/g)	iH_c (Koe)
0.15	650	36.19	20.82	1.795
"	750	37.13	21.15	1.950
"	850	37.43	21.43	2.800
"	925	37.84	21.36	3.000
"	1000	37.97	20.31	4.100
"	1050	52.28	31.32	4.150
"	1100	54.88	32.03	2.800
"	1150	55.25	25.50	2.600
"	1200	55.42	33.01	2.100
0.75	925	75.00	44.52	3.850
0.25	925	67.92	40.22	3.100
0.08	925	58.39	31.63	4.000
0.02	925	56.45	31.61	3.700

Table 1Zi Effect of ferritization temperature on magnetic property

Coprecipitate pressed and ferritized

Dilution (mol Fe)	Ferritization temperature (C)	σ_s (emu/g)	σ_r (emu/g)	iH_c (KOe)
0.15	650	18.76	11.07	1.908
"	750	24.90	14.10	2.100
"	850	27.37	15.43	2.450
"	925	32.20	19.36	3.000
"	1000	37.74	21.93	4.100
"	1050	38.07	20.09	4.150
"	1100	47.92	28.26	3.650
"	1150	48.99	28.81	2.190
"	1200	50.00	29.50	2.600
0.75	925	65.01	37.25	2.600
0.25	925	55.78	33.00	3.610
0.08	925	54.23	28.28	3.400
0.02	925	50.17	29.93	3.220

Table 18: Magnetization and demagnetization data

Coprecipitates directly ferritized		σ (emu/g)								
Ferritization temperature (°C)	Field (kOe)	650	750	850	925	1000	1050	1100	1150	1200
0	0	4.35	4.48	4.66	5.13	5.16	6.26	6.51	6.75	1.67
1	12.67	12.99	13.35	13.47	14.69	19.44	20.69	20.00	20.24	
2	18.78	19.31	19.72	20.14	21.56	28.94	31.39	31.50	30.12	
3	22.72	23.45	23.91	24.35	25.47	34.77	37.67	38.50	36.14	
4	26.39	27.13	27.64	27.89	28.59	39.31	42.32	43.00	41.20	
5	29.66	30.23	30.75	31.02	31.25	43.20	45.81	46.50	45.54	
6	31.97	32.64	33.07	33.33	33.44	46.22	48.84	49.25	48.92	
7	33.61	34.37	34.78	35.10	35.16	48.60	50.93	51.50	51.57	
8	34.97	35.86	36.18	36.59	36.56	50.54	53.02	53.50	53.73	
9	36.19	37.13	37.45	37.84	37.97	52.28	54.88	55.25	55.42	
10	35.10	35.98	36.34	36.59	36.72	50.54	53.02	53.50	53.73	
11	34.59	34.94	35.37	35.51	35.51	48.81	51.16	51.50	51.81	
12	33.80	33.22	33.54	33.88	33.91	46.87	49.06	49.25	49.88	
13	32.52	31.72	32.14	32.38	32.50	44.71	46.74	46.75	47.71	
14	30.52	30.11	30.43	30.75	30.78	42.55	44.42	43.75	45.30	
15	27.89	28.39	28.73	28.98	28.91	40.17	41.86	40.00	42.89	
16	26.12	26.24	26.86	26.94	27.03	37.58	39.06	34.50	40.24	
17	23.95	24.25	24.69	24.63	24.53	34.56	35.81	25.50	37.11	
18	20.88	21.15	21.43	21.36	20.31	31.32	32.09	12.25	33.01	

Table 19: Magnetization and demagnetization data
Coprecipitates pressed and subsequently ferritized

Ferritization temperature (C) Field (kOe)	σ (emu/g)						
	650	750	850	925	1000	1050	1100
0	2.29	4.67	7.86	1.61	7.43	0.45	5.74
1	4.67	7.14	11.79	4.80	12.85	5.89	12.34
2	8.42	9.24	17.18	7.89	19.10	10.42	21.23
3	11.34	13.45	19.80	16.26	23.82	20.09	28.69
4	13.54	16.56	21.54	21.88	27.59	26.59	34.58
5	15.90	18.66	22.99	25.77	30.78	30.97	39.31
6	16.38	20.13	24.31	28.24	33.77	33.53	42.47
7	17.38	21.13	25.47	29.85	35.14	35.34	44.62
8	18.12	22.05	26.19	31.19	36.56	36.71	46.34
9	18.76	24.90	27.37	32.20	37.74	38.07	47.92
10	18.12	22.14	26.64	31.23	36.67	36.85	46.48
11	17.47	21.32	25.62	30.15	35.49	35.50	44.91
12	16.83	20.49	24.60	28.96	34.43	34.13	43.33
13	16.10	19.58	23.44	27.72	33.02	32.47	41.61
14	15.27	18.57	22.27	26.41	31.60	30.81	39.60
15	14.46	17.57	20.96	25.00	29.95	29.00	37.30
16	13.45	16.38	19.65	23.42	28.18	26.88	35.15
17	12.44	15.28	17.90	21.63	25.82	24.32	32.28
18	11.07	14.10	15.43	19.36	21.93	20.09	28.81
19							28.26
20							29.50

Table 20 : Magnetization and demagnetization data

Coprecipitation at varying dilutions and ferritization
at 925°C.

	Dilution (moles Fe)	0.75	0.25	0.15	0.08	0.02
	Field (kOe)	σ (emu/g)				
0	15.12	1.82	1.61	2.73	4.01	
1	23.70	11.55	4.80	12.16	7.86	
2	39.50	20.63	7.89	18.03	11.87	
3	46.50	26.34	16.26	27.32	15.38	
4	50.34	30.53	21.88	35.38	26.92	
5	53.95	41.25	25.77	42.62	35.62	
6	56.88	47.52	28.24	47.68	41.81	
7	60.27	51.16	29.85	50.68	45.82	
8	62.75	53.79	31.19	52.60	48.33	
9	65.01	55.78	32.20	54.23	50.17	
8	62.98	53.96	31.23	52.73	48.66	
7	60.72	52.15	30.15	51.23	46.82	
6	58.24	50.17	28.96	49.45	44.98	
5	55.76	48.02	27.72	47.54	42.98	
4	53.05	45.71	26.41	45.49	40.80	
3	50.11	43.23	25.00	43.17	38.46	
2	46.73	40.59	23.42	40.44	36.12	
1	42.89	37.46	21.63	36.48	33.28	
0	37.25	33.00	19.36	28.28	29.93	

Table 21 : Magnetization and demagnetization data

Coprecipitation at varying dilutions and ferritization
at 925°C and pressed.

	Dilution (moles Fe)	0.75	0.25	0.15	0.08	0.02
	Field (kOe)	σ (emu/g)				
0	0	8.57	8.26	5.16	8.03	6.77
1	26.19	24.35	14.65	24.57	21.93	
2	40.23	36.53	21.56	35.52	33.23	
3	48.81	44.14	25.47	41.61	39.52	
4	55.95	50.45	28.59	45.74	43.87	
5	61.90	55.66	31.25	49.15	47.26	
6	66.43	59.58	33.44	51.82	50.00	
7	69.76	62.62	35.16	54.26	52.42	
8	72.62	65.23	36.56	56.45	54.52	
9	75.00	67.42	37.97	58.39	56.45	
8	72.62	65.23	36.72	56.45	54.22	
7	70.23	62.84	35.31	54.26	52.58	
6	67.14	60.45	33.91	52.07	50.32	
5	64.05	57.62	32.50	49.63	47.90	
4	60.95	54.79	30.78	46.96	45.48	
3	57.38	51.75	28.91	44.04	42.74	
2	53.57	47.83	27.03	40.63	39.68	
1	49.52	44.57	24.63	34.74	36.13	
0	44.52	40.22	21.36	31.63	31.61	

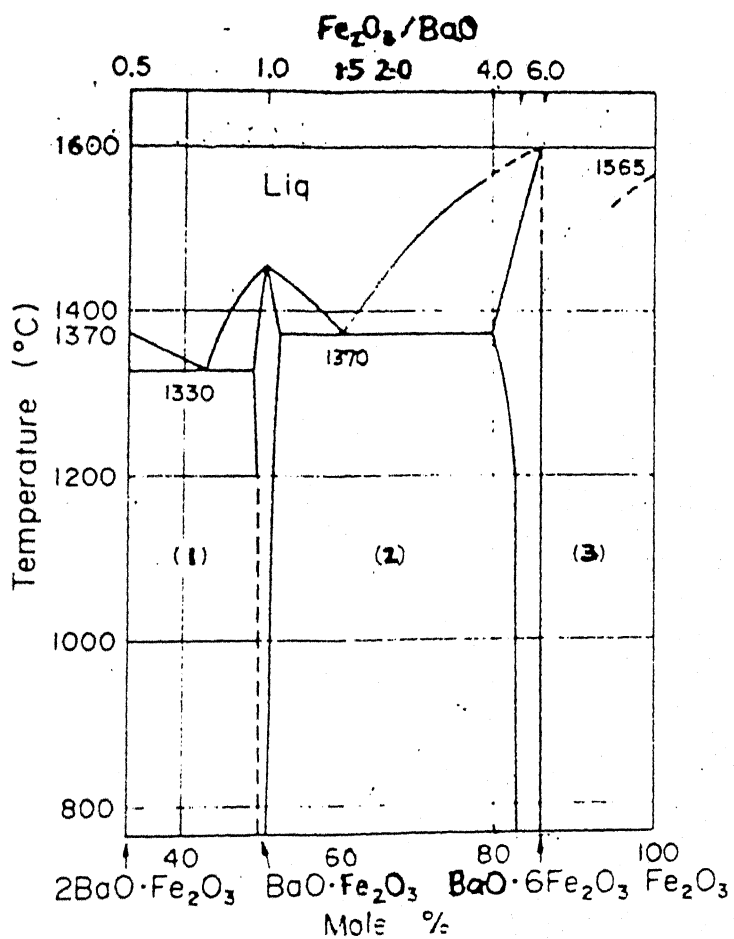


Fig. 1 Phase diagram of $\text{BaO}-\text{Fe}_2\text{O}_3$ system at $\text{PO}_2 = 1/5 \text{ atm.}$ in solid phase region and at $\text{PO}_2 = 1 \text{ atm.}$ in liquid phase region. (1) $2\text{BaO}\cdot\text{Fe}_2\text{O}_3 + \text{BaO}\cdot\text{Fe}_2\text{O}_3$, (2) $\text{BaO}\cdot\text{Fe}_2\text{O}_3 + \text{BaO}\cdot 6\text{Fe}_2\text{O}_3$, (3) $\text{BaO}\cdot 6\text{Fe}_2\text{O}_3 + \text{Fe}_2\text{O}_3$ (Ref. Kojima, H., "Fundamental properties of hexagonal ferrites with magnetoplumbite structure", in "Ferromagnetic materials, Vol. 3", Ed. Wohlfarth, E.P., North-Holland, 1982, p.310).

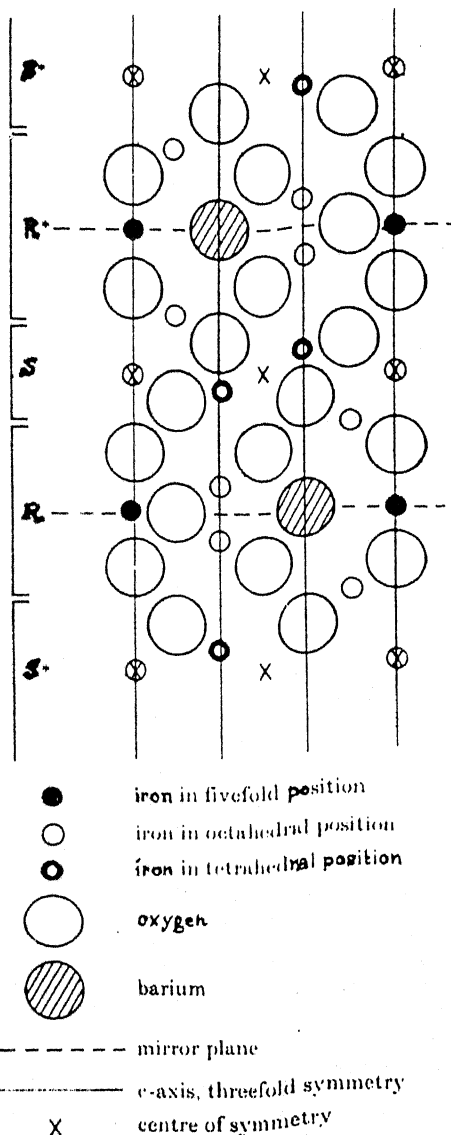
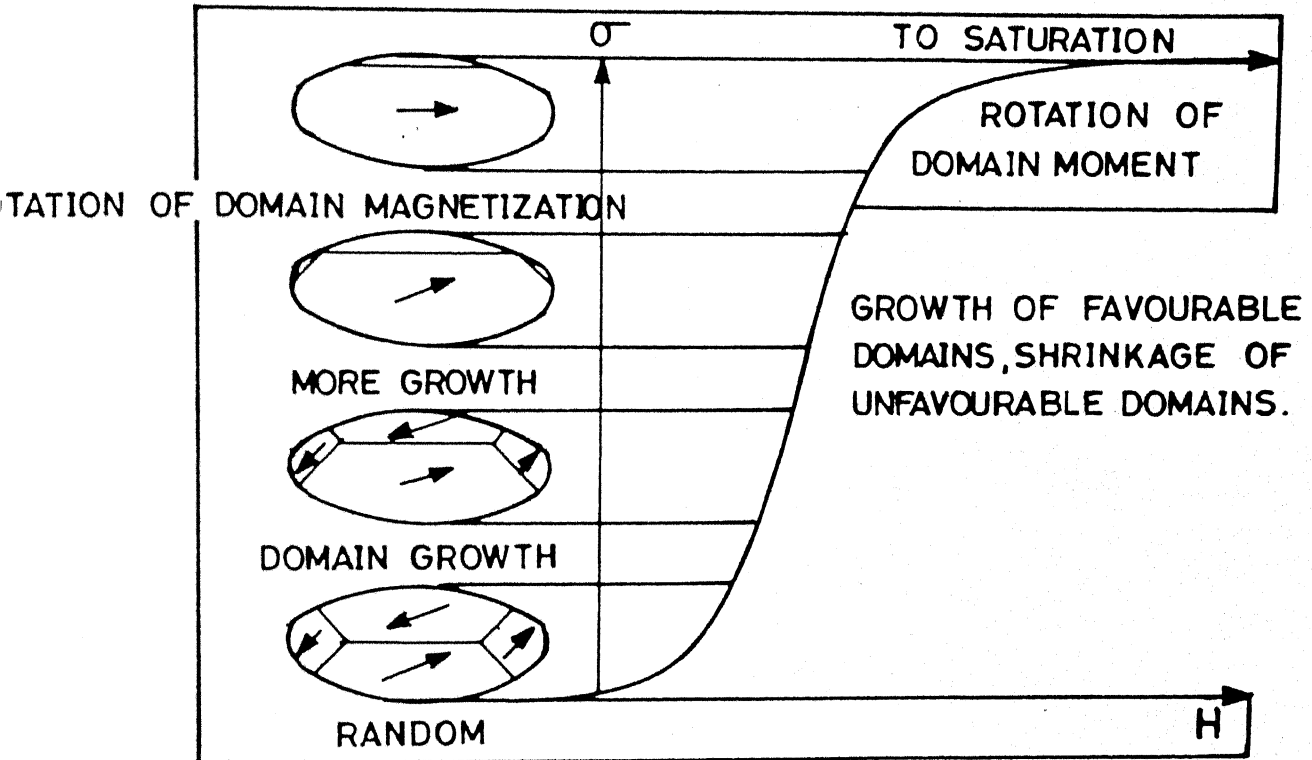
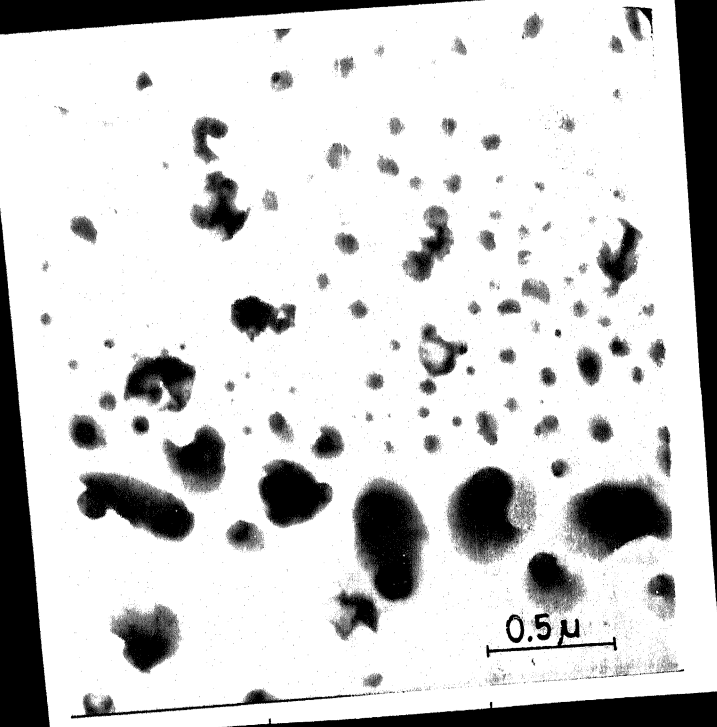


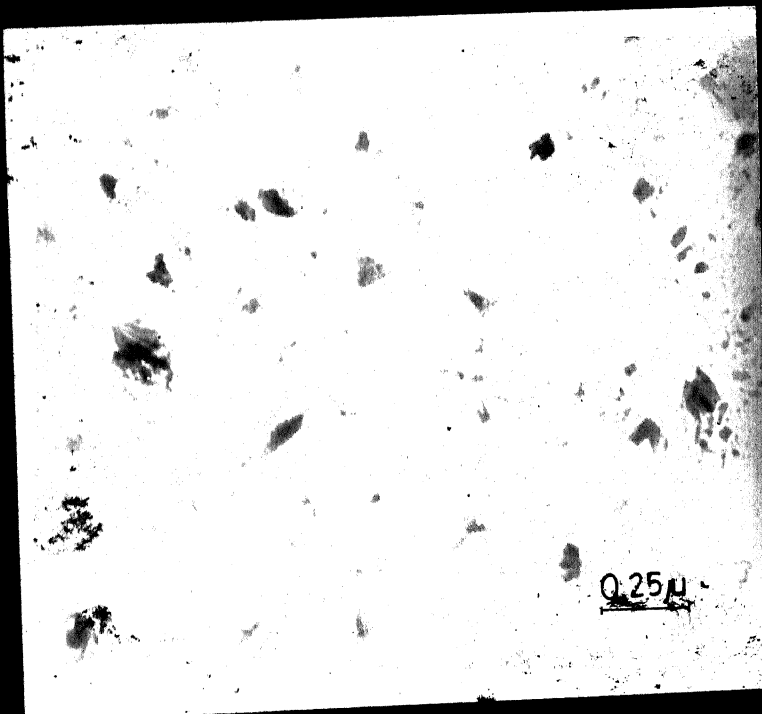
Fig. 2: The unit cell of $\text{BaO} \cdot 6\text{Fe}_2\text{O}_3$ including ferric ion moment directions (Ref. Standly, K.J., "Oxide magnetic materials", Clarendon Press, 1972, p. 37).



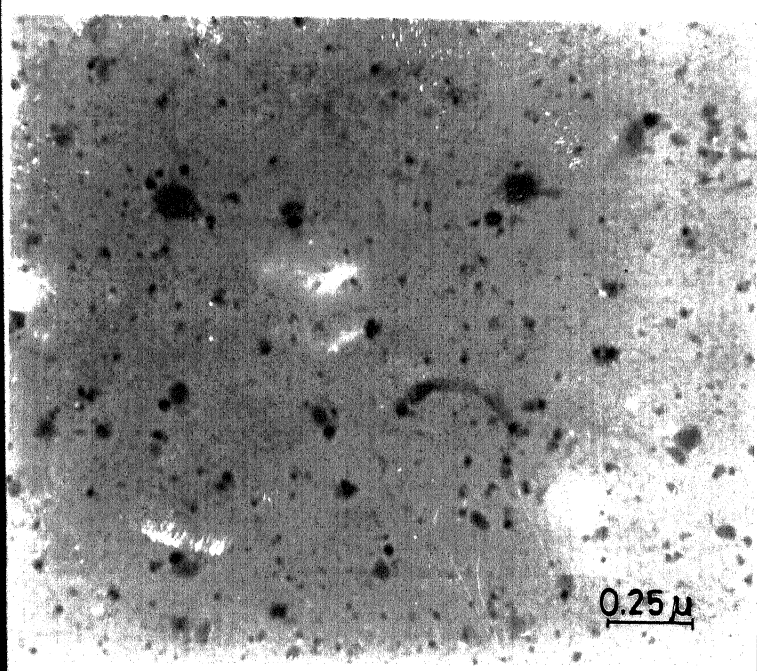
g. 3 : Domain growth and rotation in ferromagnetic material and associated magnetization curve (Ref. Rose, R.M., Shepard, L.A. and Wulff, J., "Structure and properties of materials, Vol. 4", Wiley Eastern, 1983, p. 193).



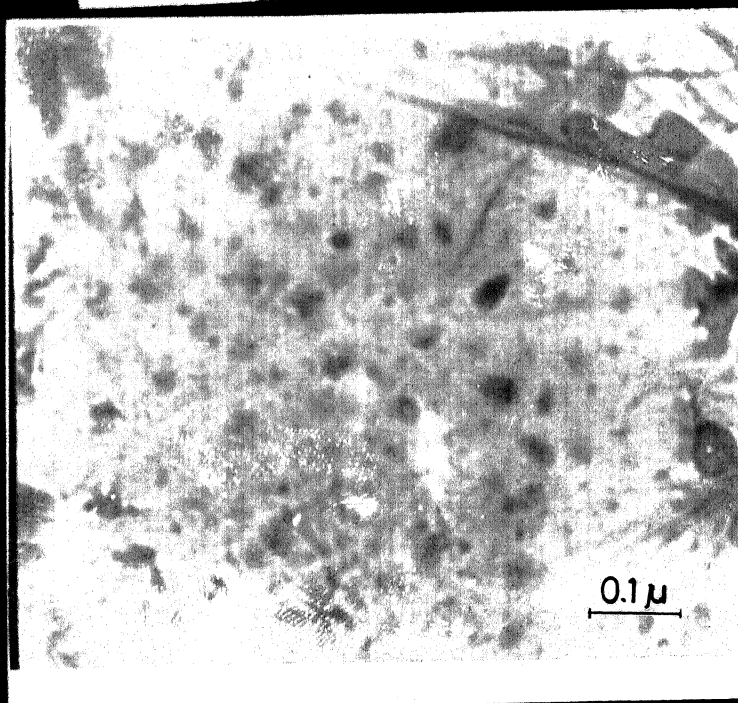
4(a) Dilution : 0.75 (M) Fe



4(b) Dilution : 0.15 (M) Fe

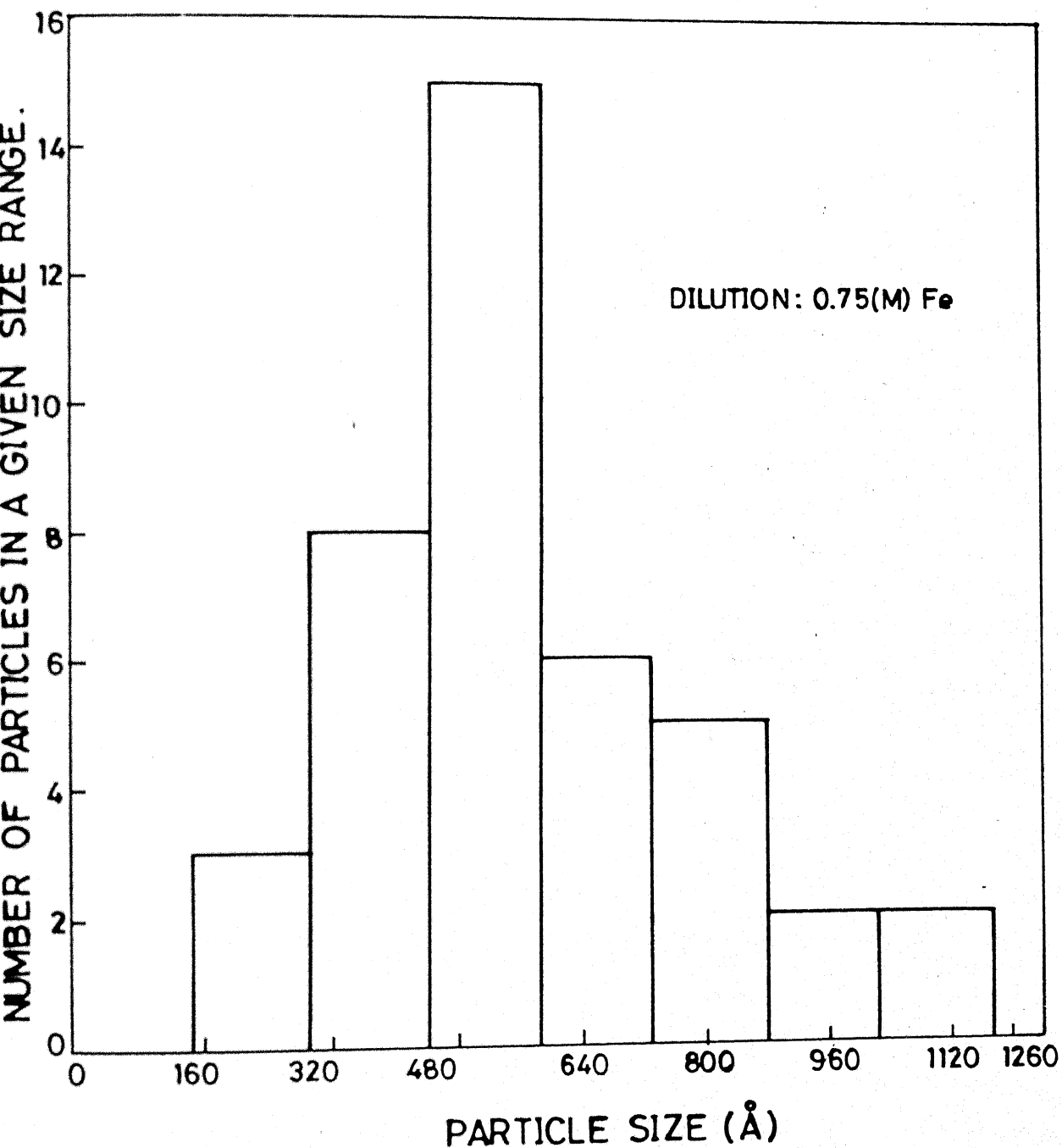


A(c) Dilution : 0.08(M) Fe



A(d) Dilution : 0.02(M) Fe

Electron micrographs showing coprecipitated particles
of Ba/Fe-complex at varying dilutions.



g.5 : Histogram showing particle size distribution of coprecipitated Ba/Fe-Complex at a dilution of 0.75 (M) Fe.

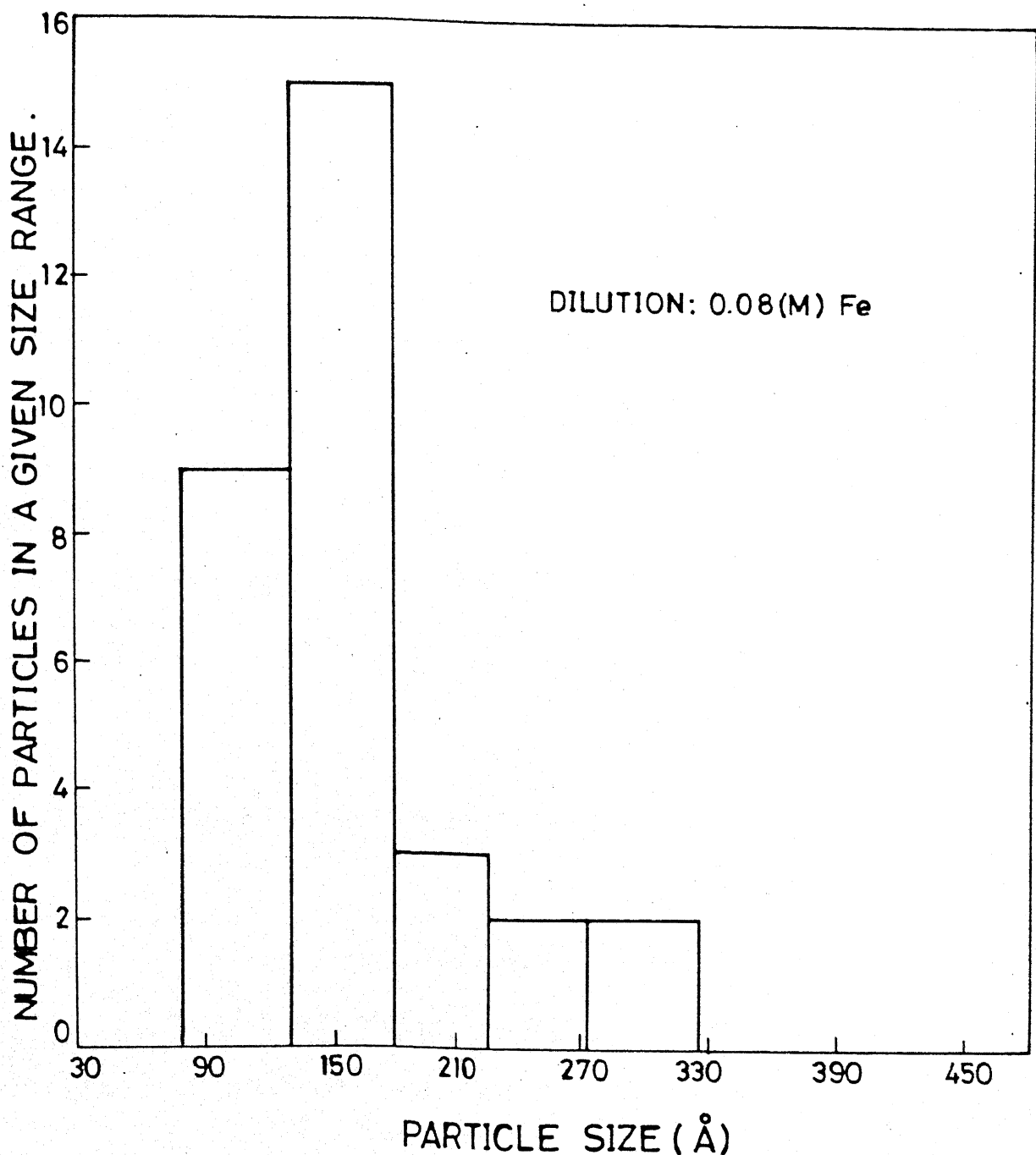


Fig. 6 : Histogram showing particle size distribution of co-precipitated Ba/Fe-complex at a dilution of 0.08 (M) Fe.

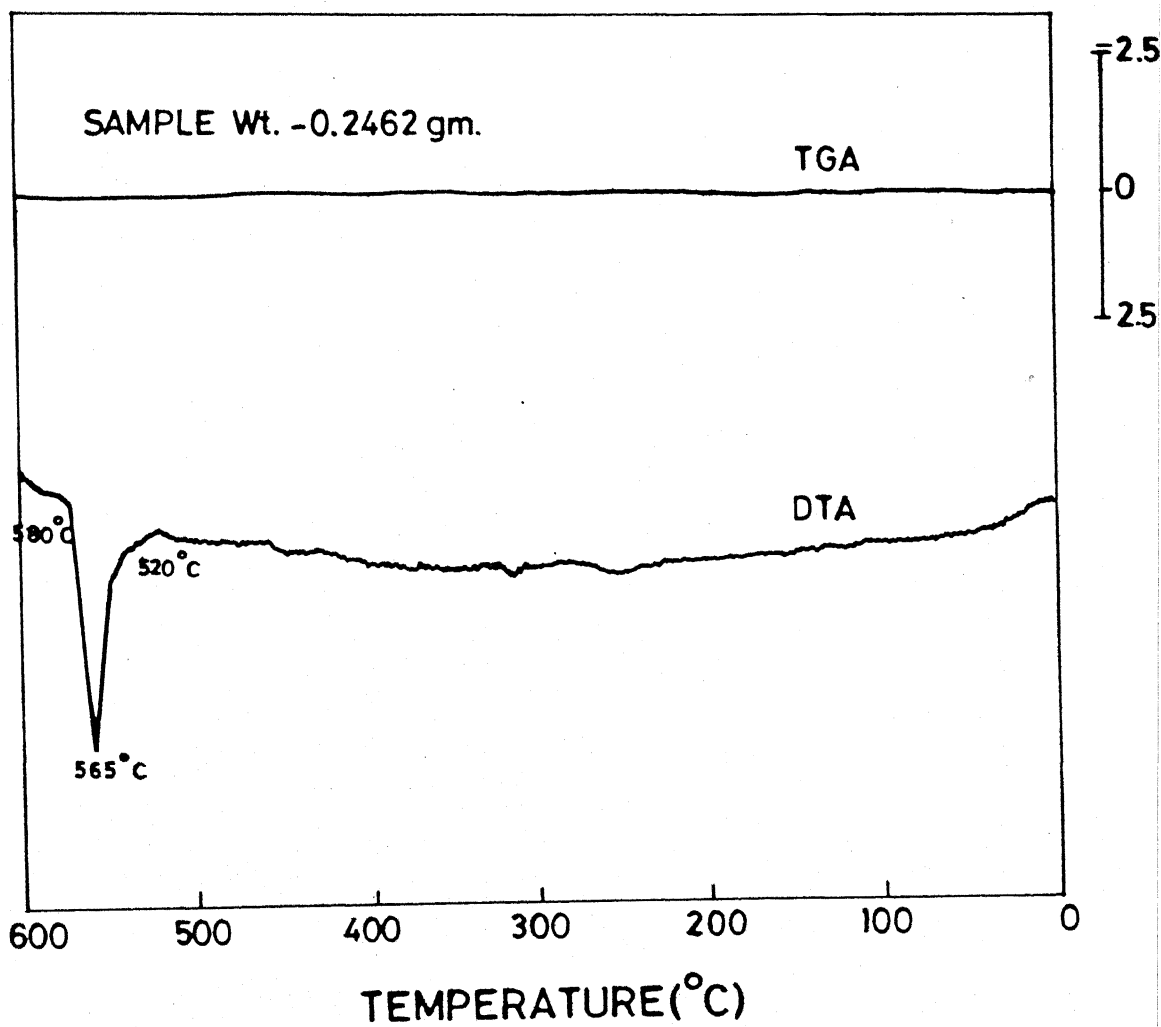


Fig. 7 : DTA and TGA curves of crystalline K_2SO_4 (particle size 115 μm).

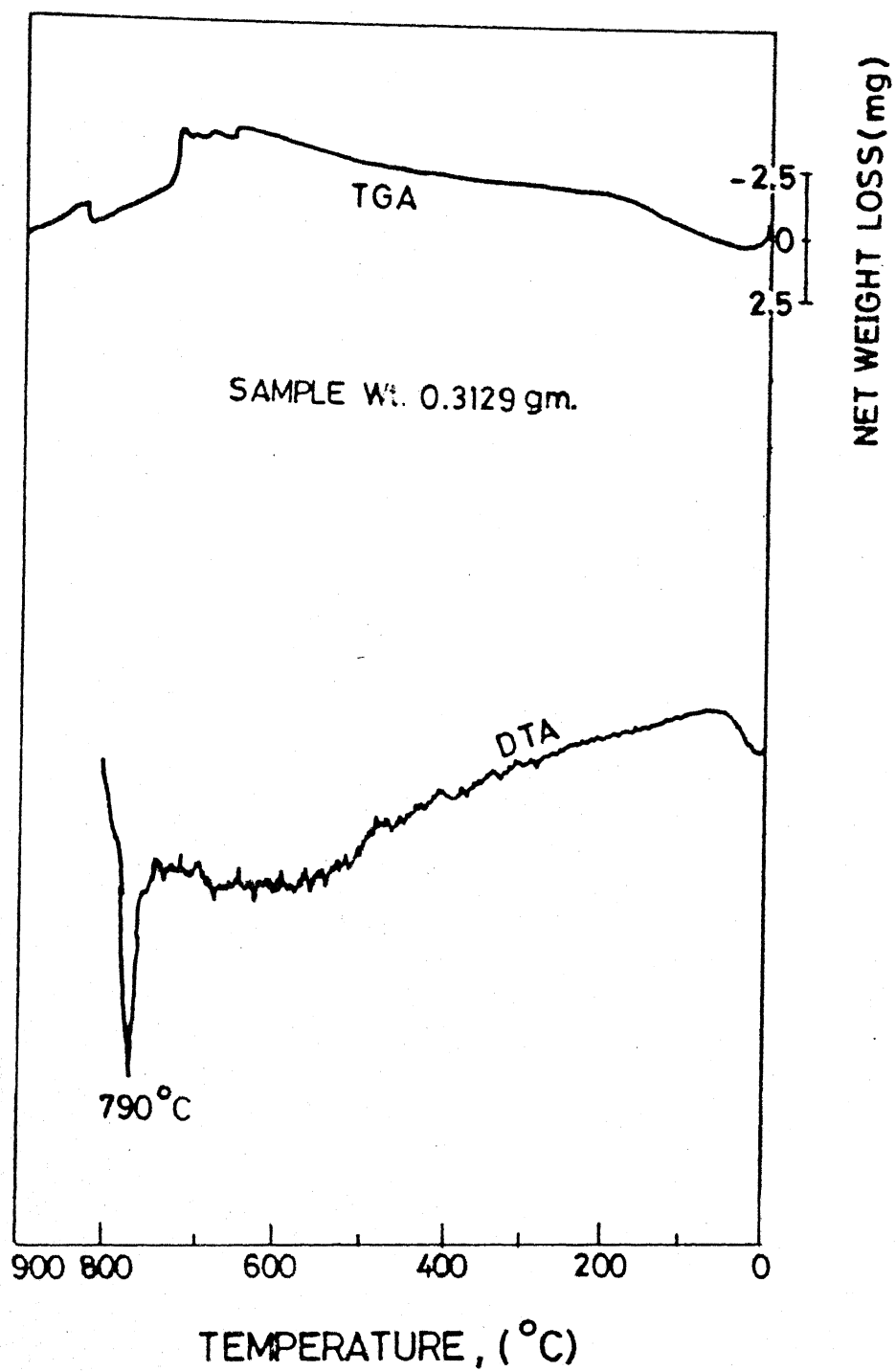


Fig. 8: DTA and TGA curves of precipitated BaCO_3 .

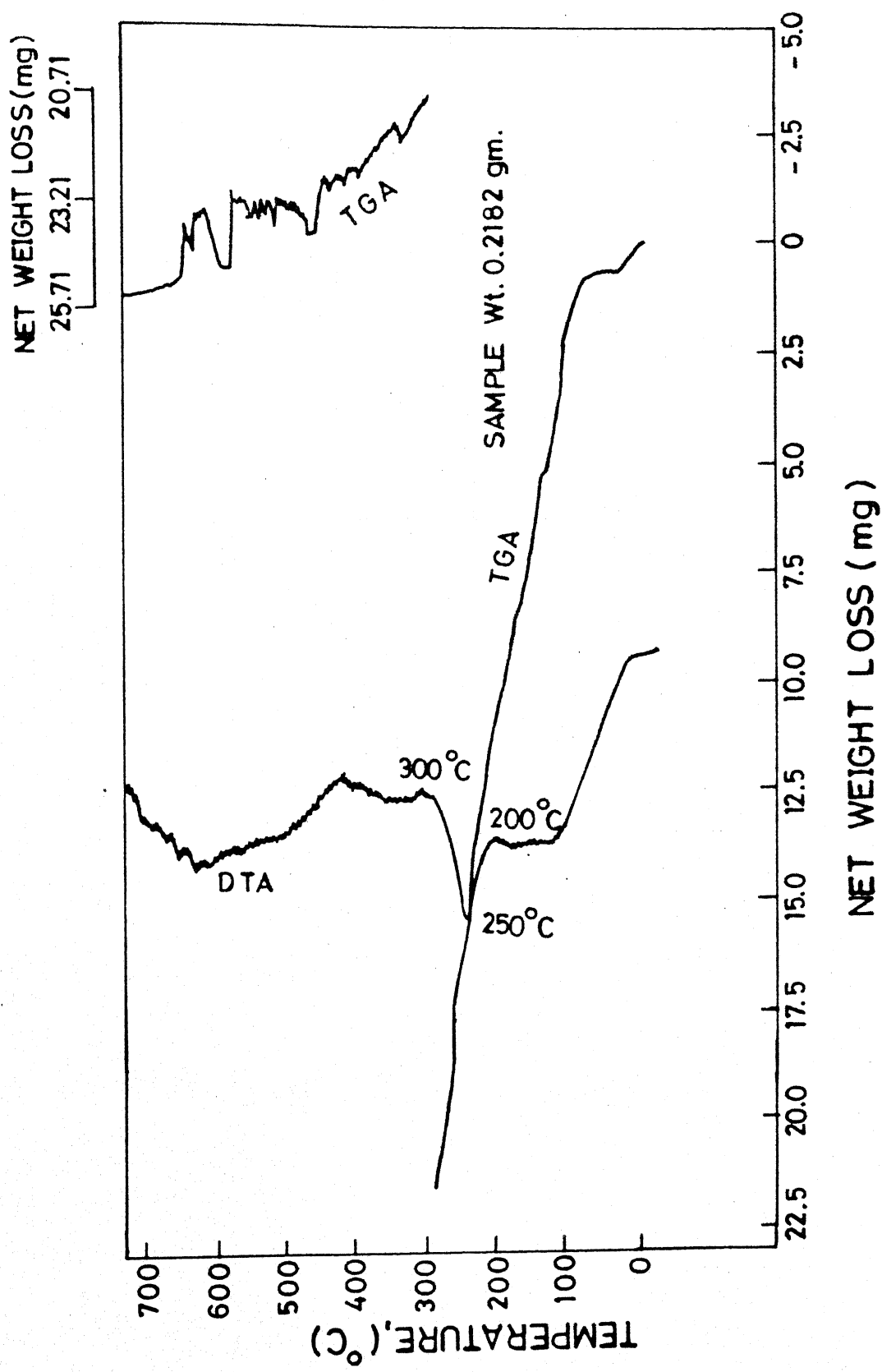


Fig. 9 DTA and TGA curves of precipitated Fe-Complex.

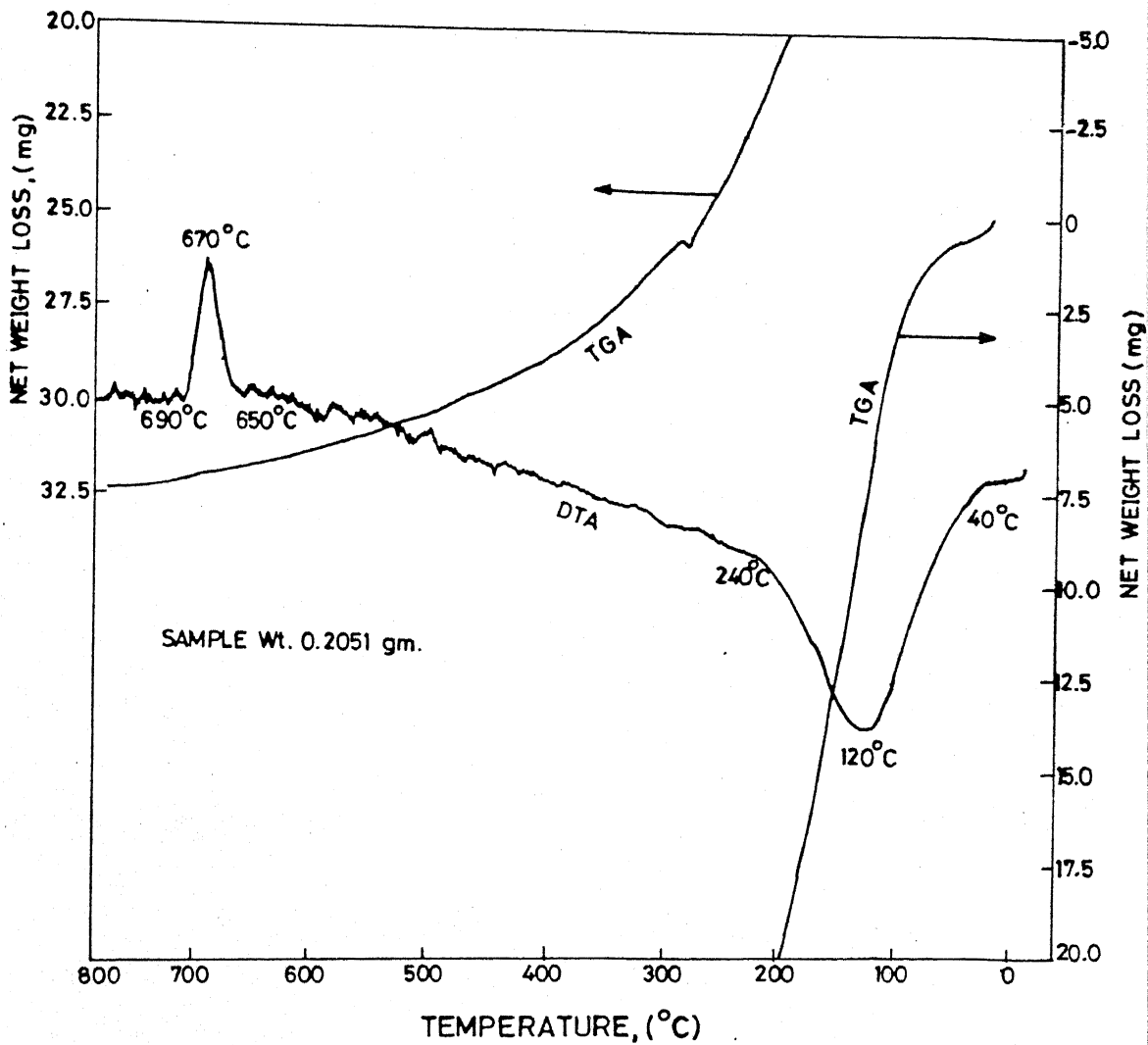


Fig. 10 : DTA and TGA curves of coprecipitated Ba/Fe-complex at dilution of 0.03 (M) Fe.

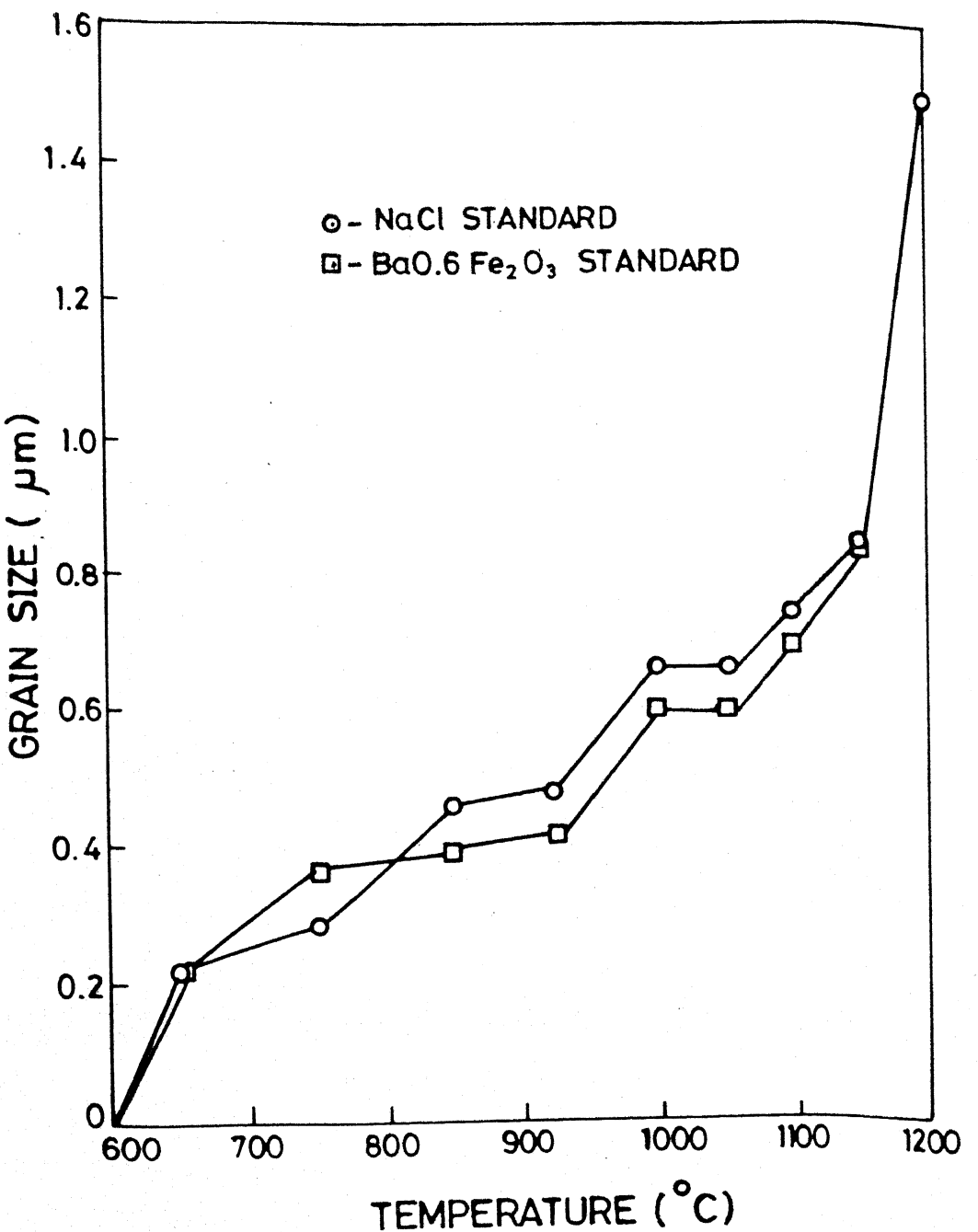


Fig. 11 : Effect of ferritization temperature on grain size of BaO · 6Fe₂O₃.

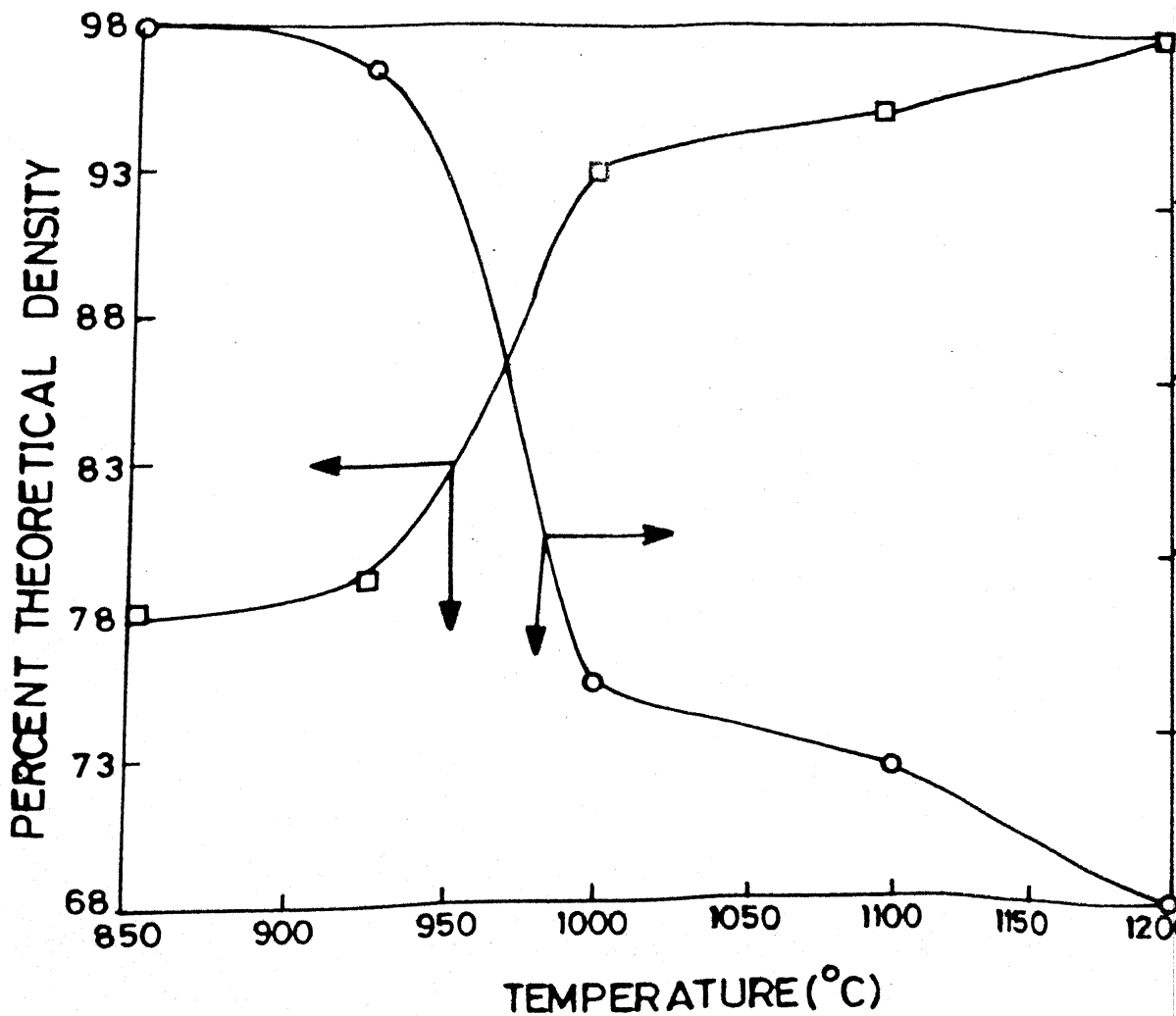


Fig. 12: Effect of pelletization temperature on density and porosity of $\text{Ba}_0.6\text{Fe}_2\text{O}_3$.

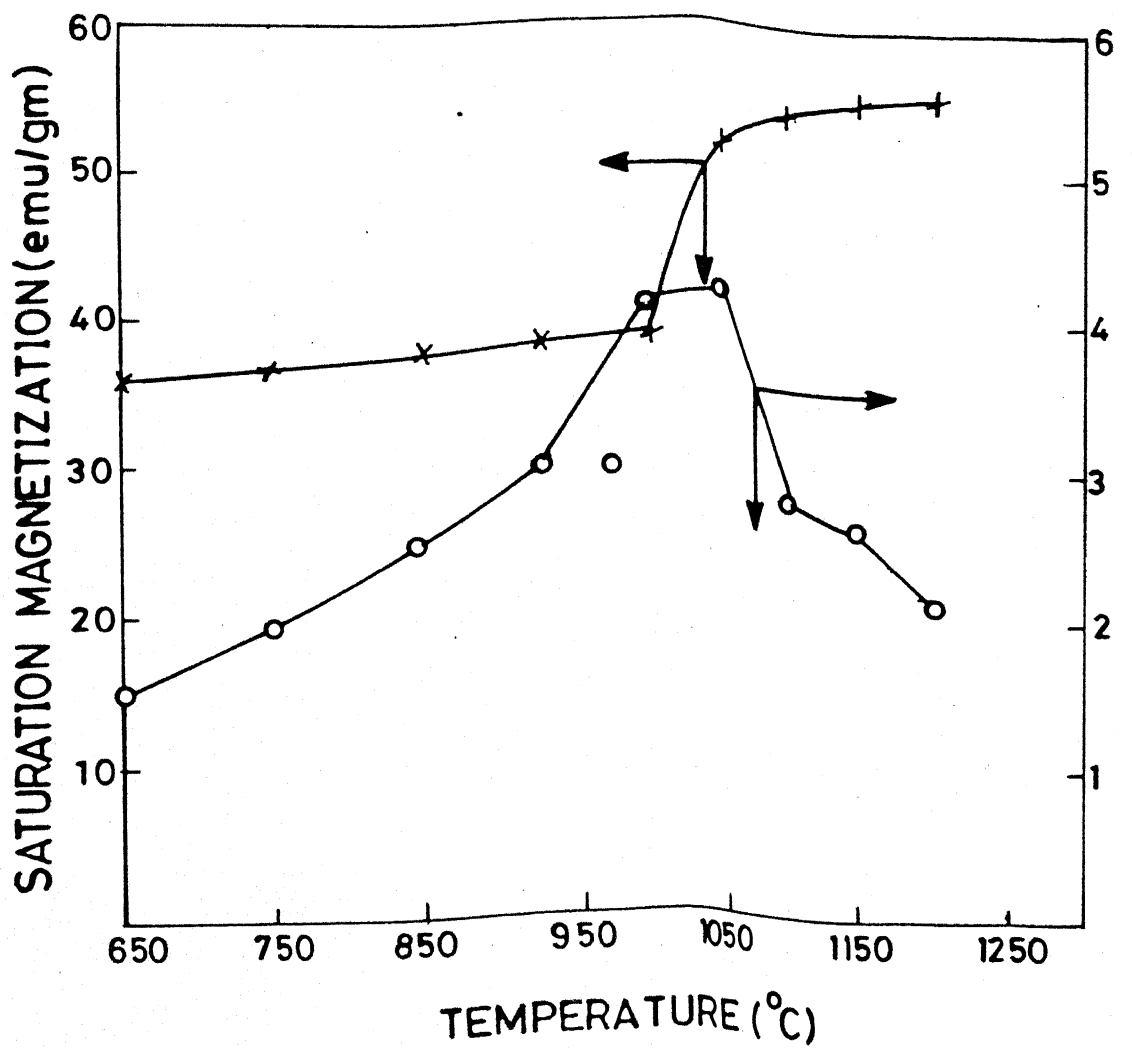


Fig. 13 : Effect of ferritization temperature on magnetic properties of directly ferritized coprecipitates.

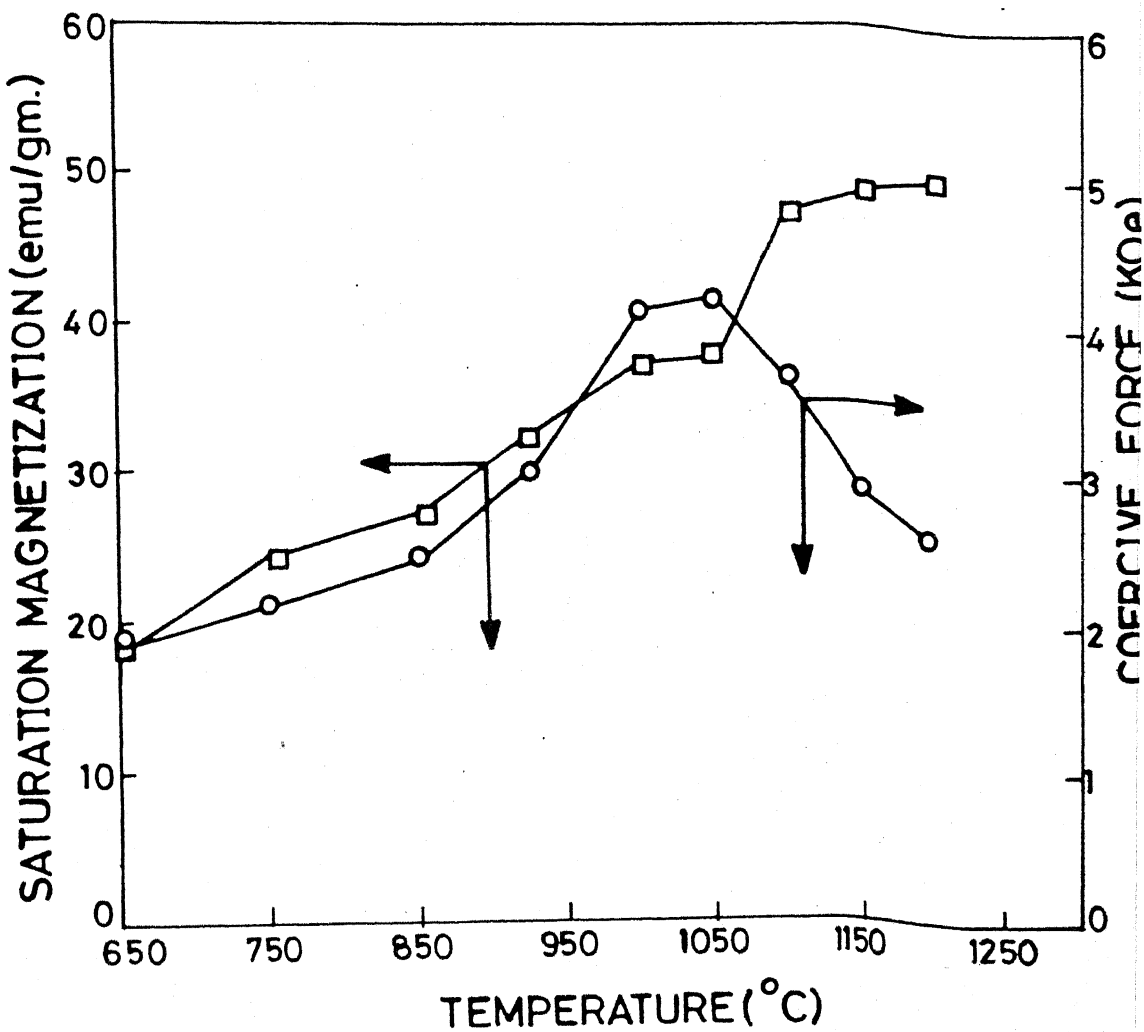


Fig. 14 : Effect of ferritization temperature on magnetic properties of pressed coprecipitates followed by ferritization.

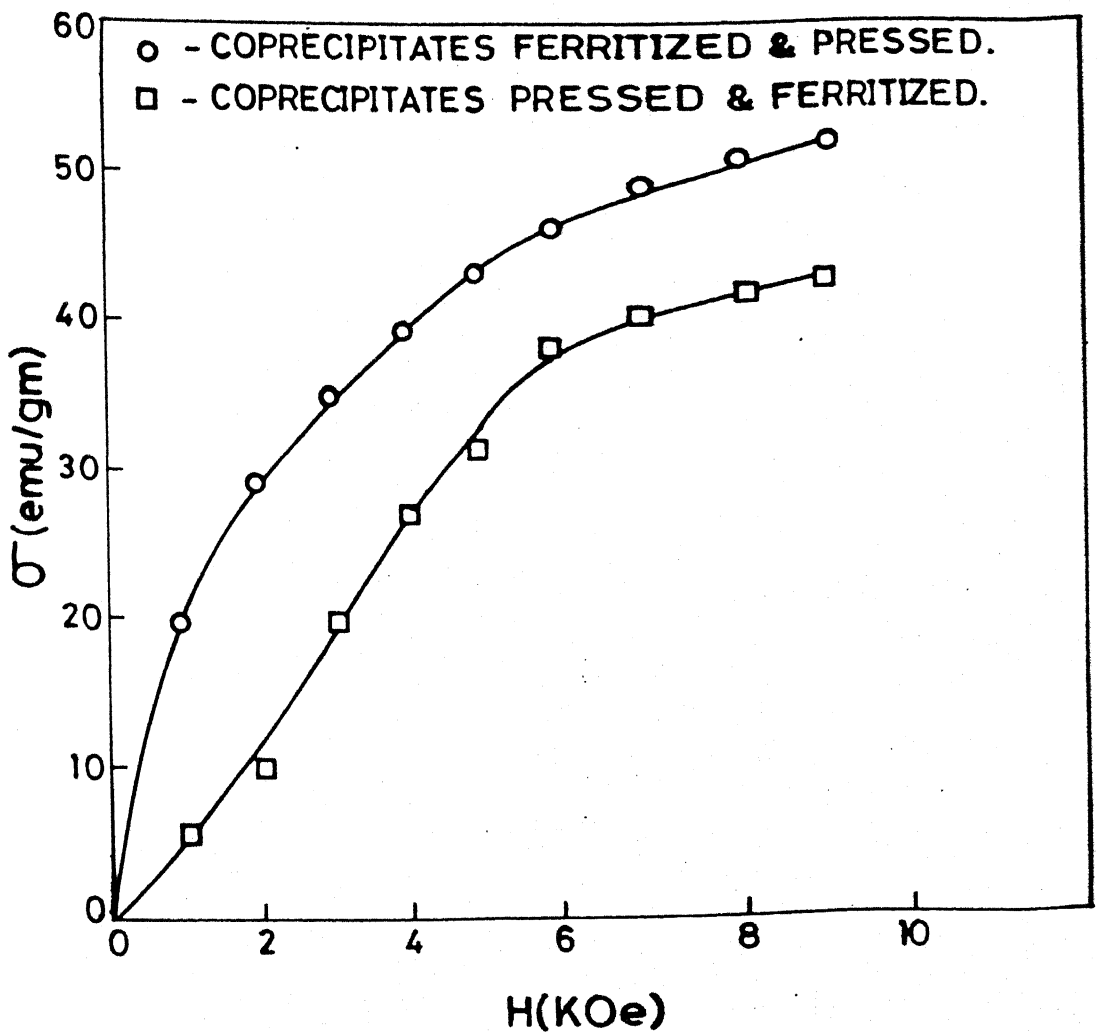


Fig. 15 : Magnetization curves of coprecipitates ferritized by different routes.

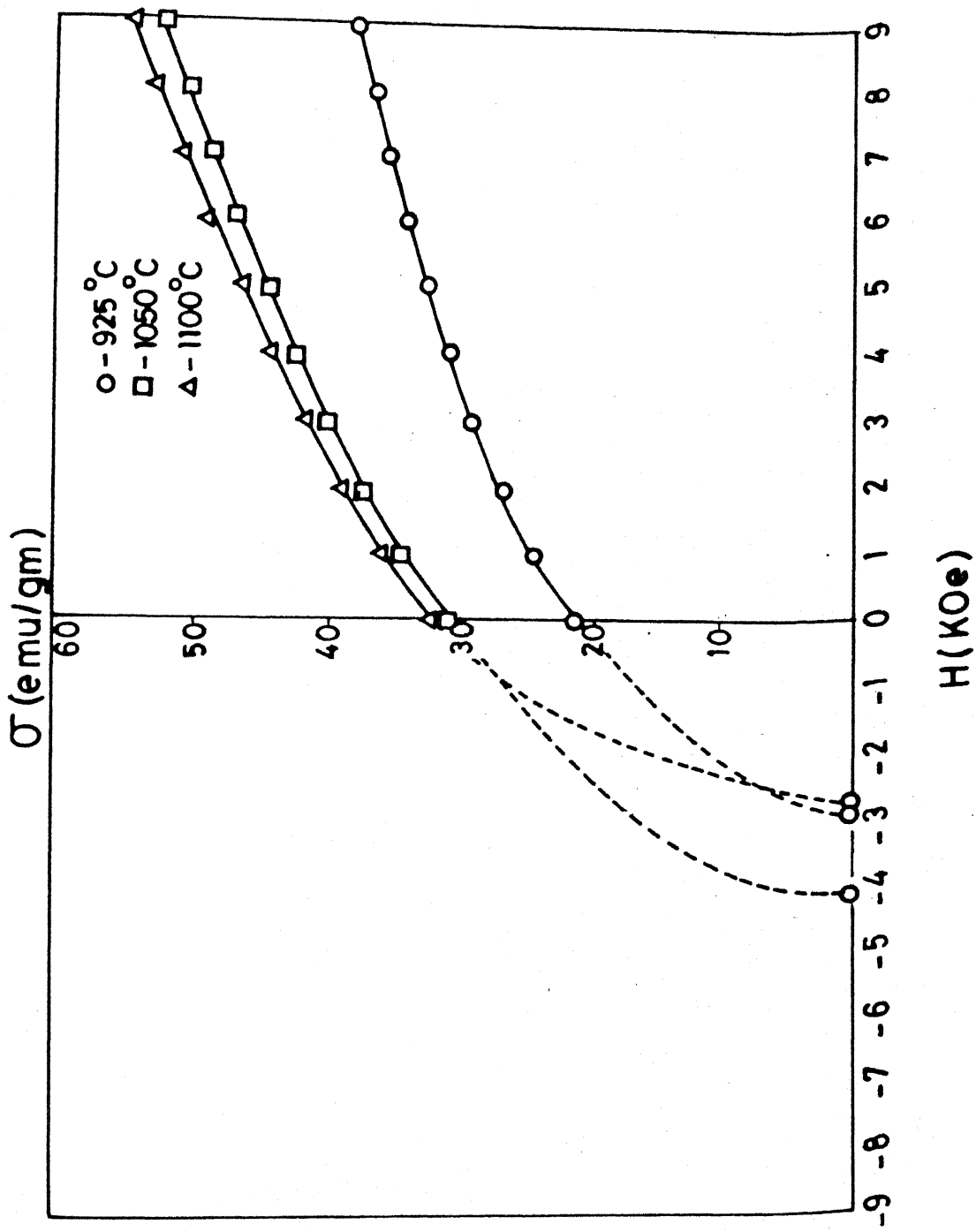


Fig. 16: Demagnetization curves of the directly ferritized coprecipitates.

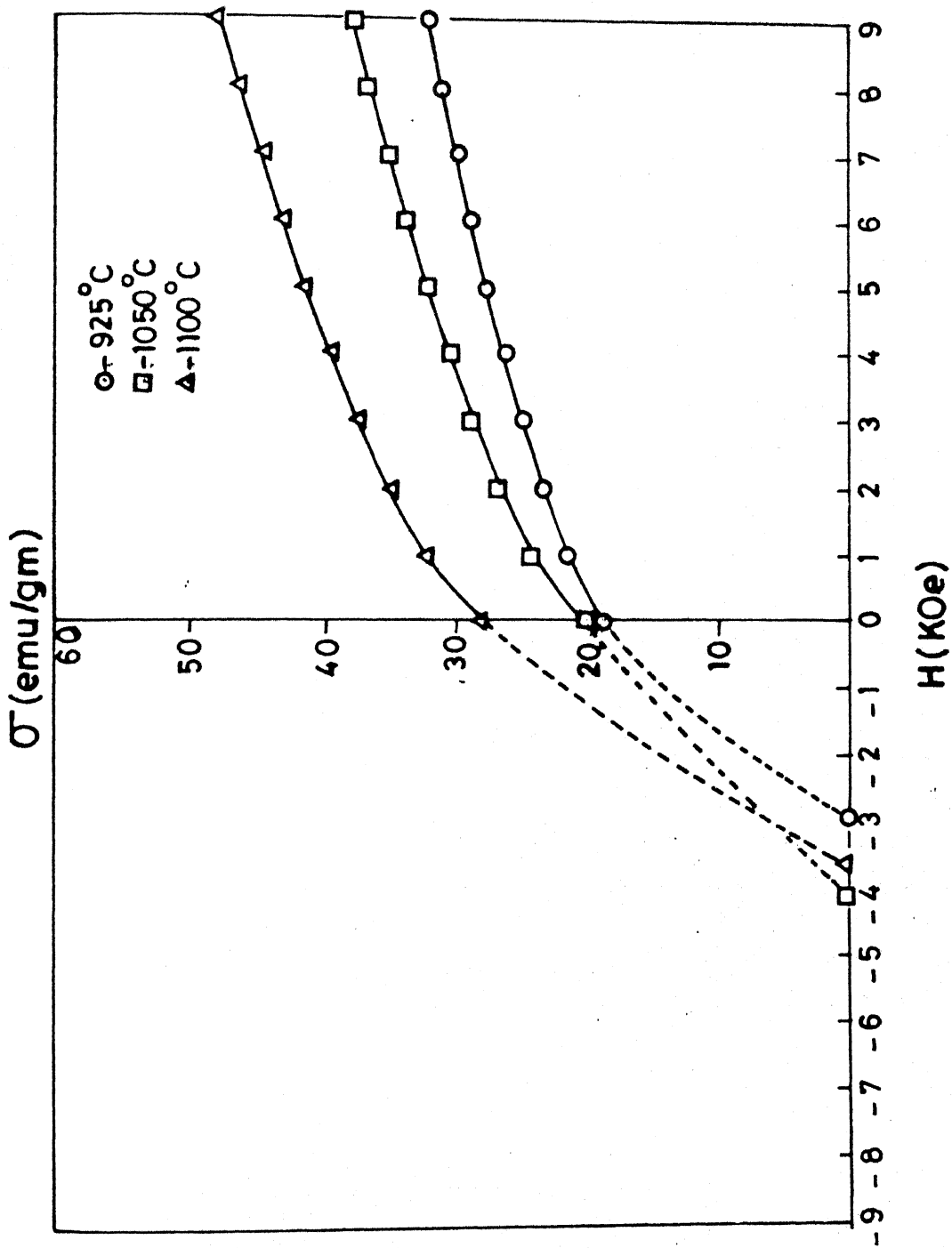


Fig. 17: Demagnetization curves of the prepressed coprecipitates followed by ferritization.

REFERENCES

1. Standly, K.J., "Oxide magnetic materials", Clarendon Press (1972),
 - (a) p. 149
 - (b) p. 36-38
 - (c) p. 151.
2. Kojima, H., "Fundamental properties of hexagonal ferrites with magnetoplumbite structure", in "Ferromagnetic materials, Vol. 3", Ed. Wohlfarth, E.P., North-Holland Pub. Co. (1982),
 - (a) p. 308-12
 - (b) p. 329-31
 - (c) p. 337
 - (d) p. 328.
3. Chikazumi, S., "Physics of magnetism", John Wiley and Sons (1964),
 - (a) p. 500-03
 - (b) p. 128.
4. Roos, R.M., Shepard, L.A. and Wulff, J., "Structure and properties of materials, Vol. 4", Wiley Eastern Ltd. (1983),
 - (a) p. 202
 - (b) p. 190
 - (c) p. 192-95.
5. Ghosh, N.K., "Preparation, characterization and magnetic property measurements of coprecipitated barium hexaferrite", M.Tech. thesis submitted to the Department of Metallurgical Engineering, I.I.T., Kanpur, 1980.
6. Kingery, W.D., Bowen, H.K. and Uhlmann, D.R., "Introduction to ceramics", John Wiley (1976), p. 1002.
7. Haneda, K., Miyakawa, C. and Kojima, H., "Preparation of high coercivity BaFe₁₂O₁₉", J. Am. Cer. Soc., Vol. 57(8), p. 354-57, 1974.
8. Roos, W., "Formation of chemically coprecipitated barium ferrite", J. Am. Cer. Soc., Vol. 67(11-12), p. 601-03, 1980.
9. Mallikarjuna, J., "Characterisation and magnetisation studies on coprecipitated strontium hexaferrite", M.Tech. thesis submitted to the Department of Metallurgical Engineering, I.I.T., Kanpur, 1984.

10. Allen, T., "Particle size measurement", Chapman and Hall (1975), p. 132-36.
11. Matyi, R.J., Schwartz, L.H. and Butt, J.B., "Particle size, particle size distribution and related measurements of supported metal catalysts", Catal. Rev.-Sci. Eng., Vol. 29(1), p. 45, 1987.
12. Natarajan, M., Das, A.R. and Rao, C.N.R., "Particle size effect and thermal hysteresis in crystal structure transformations", Trans. Farad. Soc., Vol. 65(563), Part-11, November, p. 3081-87, 1969.
13. Cullity, B.D., "Elements of X-ray diffraction", Addison-Wesley Co. (1956), p. 98-99, 261-62.
14. Gilreath, S.E., "Qualitative analysis using semimicro methods", McGraw-Hill (1954), p. 213, 219.
15. "Powder diffraction file, inorganic phases", JCPDS, International Centre for Diffraction Data (1985), File No.:
(a) 16-653
(b) 25-1477
(c) 20-132
(d) 27-1028.
16. Weast, R.C. (Editor), "CRC handbook of chemistry and physics", CRC Press (1980), p. B242.

APPENDIXESTIMATION OF IRON IN FERRIC CHLORIDE SOLUTION *

About 20 gm of $\text{FeCl}_3 \cdot 6\text{H}_2\text{O}$ crystal was dissolved in 500 ml of distilled water. 10 ml of the solution was transferred to a 500 ml conical flask and 10 ml of concentrated HCl was added to it. The solution was heated nearly to boiling. Concentrated stannus chloride solution was added drop by drop from a burette until the yellow colour of the solution nearly disappears. Then diluted stannus chloride solution 2 drops in excess was added until the solution gets a faint green colour, quite free from any yellow tint. The solution was then rapidly cooled under water with protection from air. The solution was then diluted to 200 ml with distilled water following 10 ml of 5% HgCl_2 addition in one portion. Then 5 ml of syrupy phosphoric acid was added to it and stirred well. Then 0.5 ml of sodium diphenyl-amine sulphonate indicator was added to it. The solution was then titrated with $(\frac{N}{10}) \text{ K}_2\text{Cr}_2\text{O}_7$ solution from a burette until a permanent end point of violet-blue is reached.

The amount of Fe in solution is calculated using the formula:

1 ml of $(\frac{N}{10}) \text{ K}_2\text{Cr}_2\text{O}_7$ solution \equiv 0.0055847 gm of Fe

Calculation:
$$\text{K}_2\text{Cr}_2\text{O}_7 \text{ consumed} = 10.6 \text{ ml}$$
$$\equiv 0.0597 \text{ gm Fe in } 10 \text{ ml}$$
$$\therefore \text{Concentration of Fe} = 0.00597 \text{ gm/ml}$$

* After Vogel, A.I., "A textbook of quantitative inorganic analysis", Longman (1960), p. 276, 294-96.

7
GGI. B95-

B 469c

Date Slip

104246

This book is to be returned on the
date last stamped.

1988-M-BNA-CNA